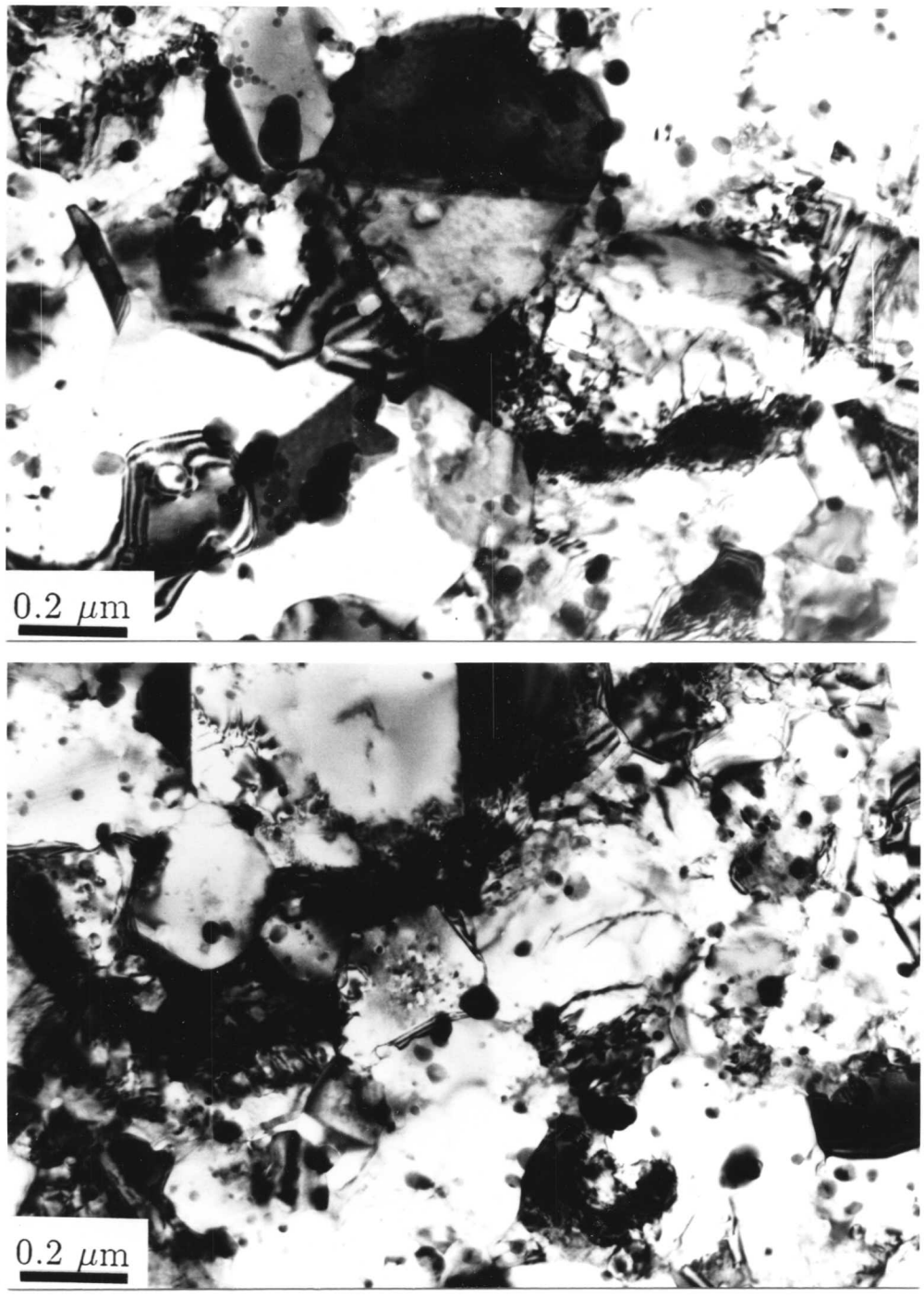

a.

b.

Figure 4.1. Electron micrographs showing the microstructure of Inconel alloy MA6000 in as-received condition. The micrographs reveal equiaxed grains in both transverse and longitudinal sections of the hot-rolled bar with a relatively low dislocation density.

a. Thin foil prepared from a transverse section of the "hot-rolled", rectangular bar.

b. Thin foil prepared from a longitudinal section (parallel to the rolling direction) of the "hot-rolled" bar.

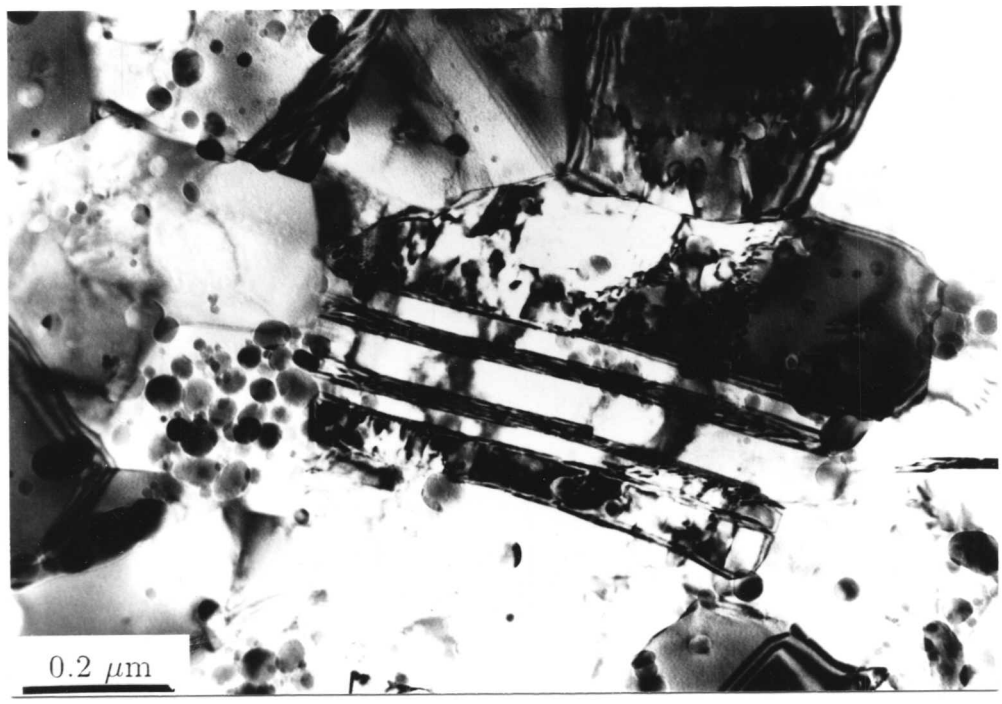

a.

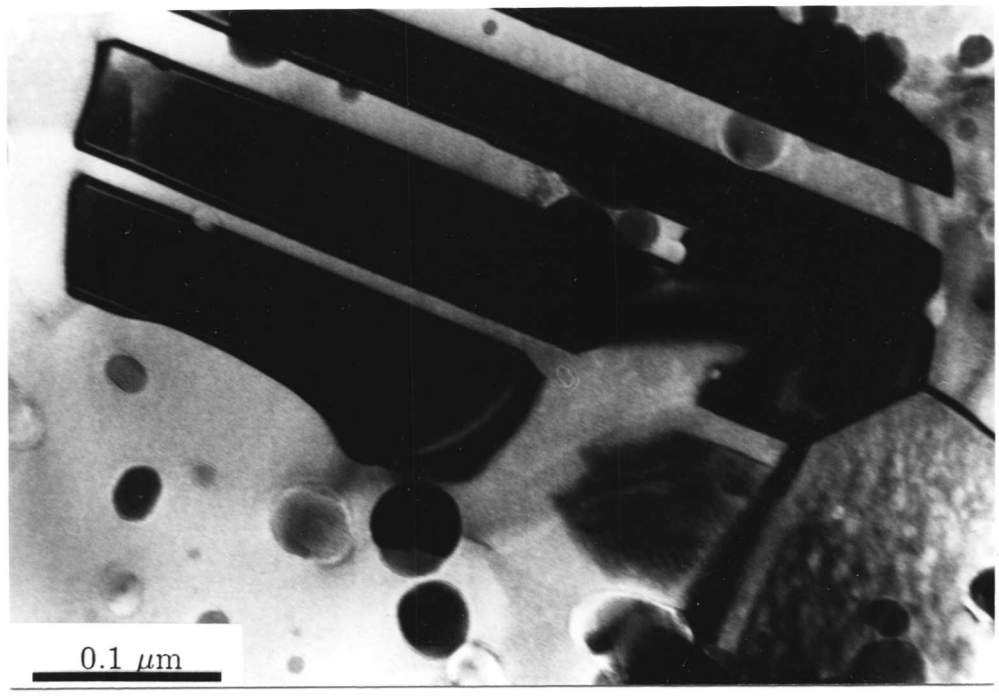

b.

Figure 4.2. Transmission electron micrographs showing annealing twins, stacking faults, and the low dislocation density of the grains in as-received Inconel alloy MA6000.

a. Bright field image recorded from the transverse section of the hot-rolled bar.

b. Bright field image recorded from the longitudinal (parallel to the rolling direction) section.

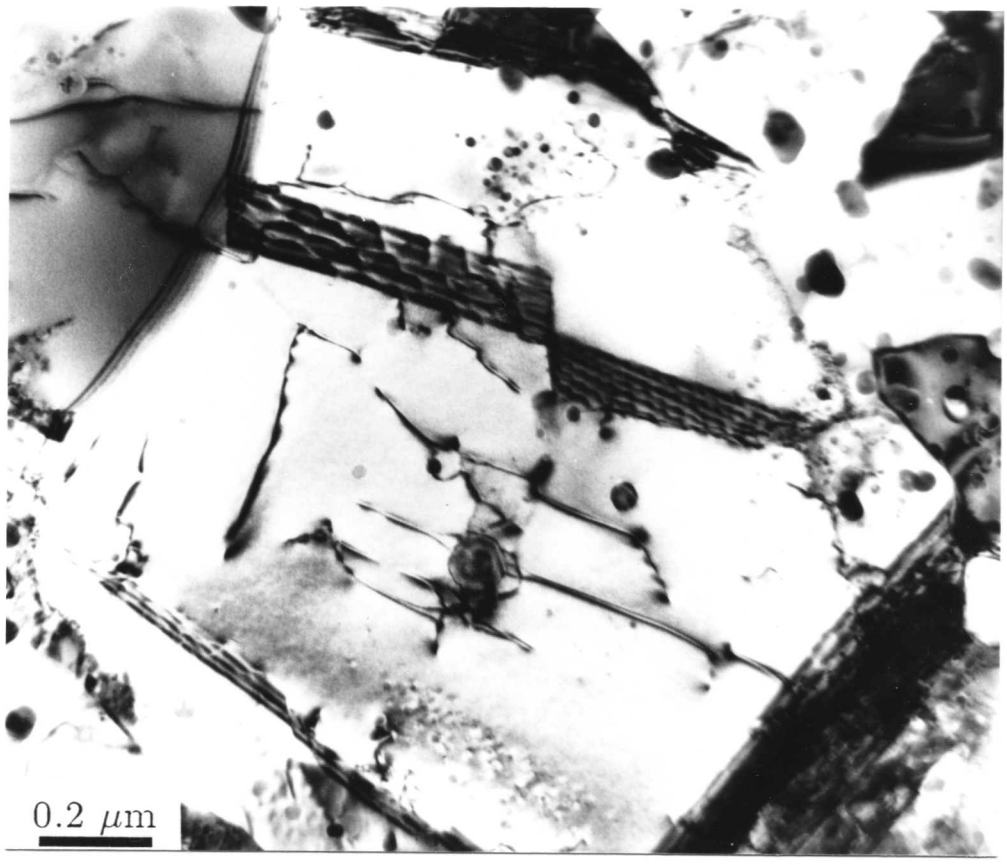

Figure 4.3. Electron micrograph showing a typical clear subgrain boundary in as-received alloy MA6000. The micrograph recorded from the foil, prepared from the longitudinal (parallel to the rolling direction) section of the as-received bar.

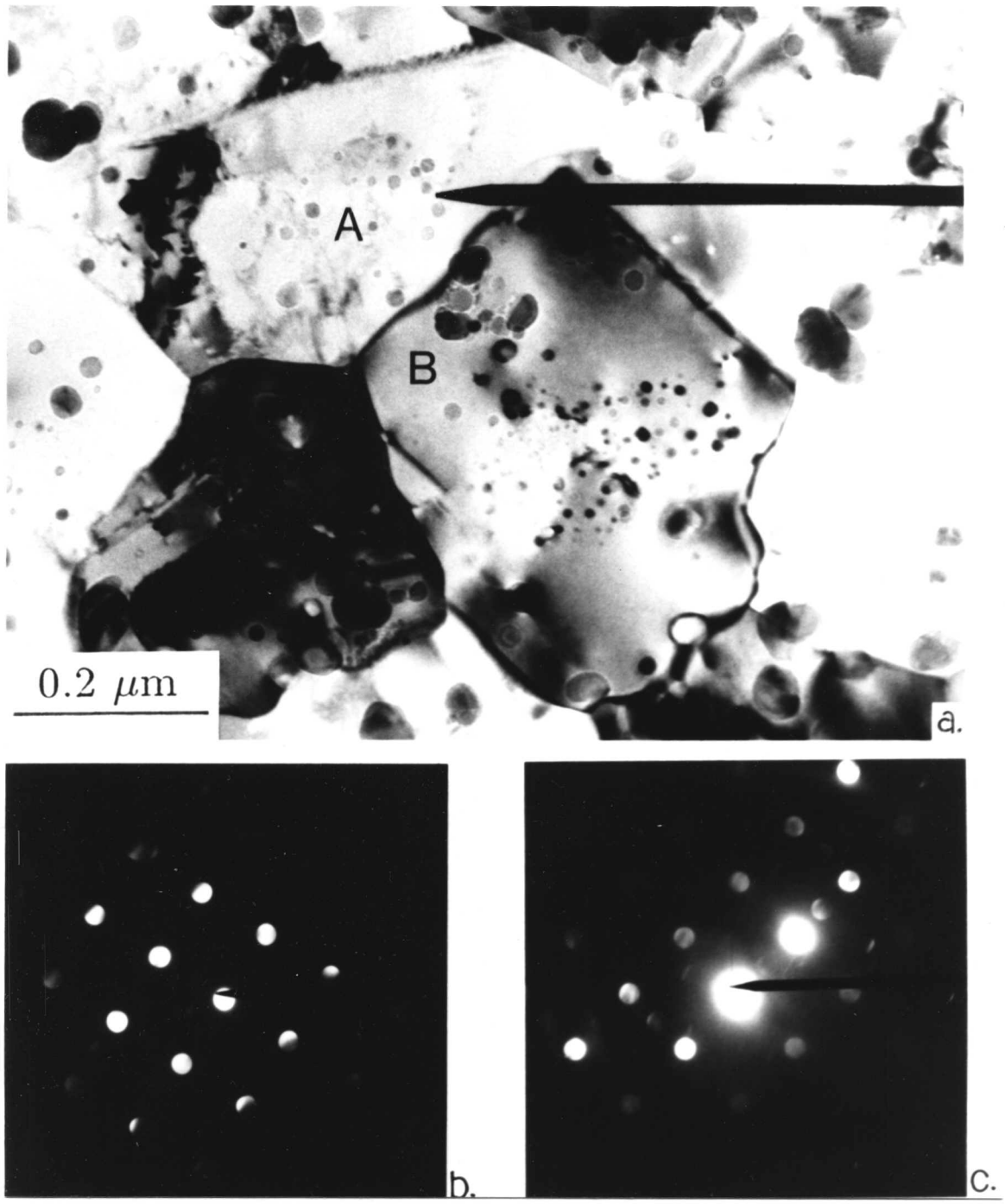

Figure 4.4. Electron micrograph and corresponding diffraction patterns from a pair of austenite grains A and B. The orientation can be represented by <0.000 0.608 0.793>/180° and this is near Σ3 orientation relationship.

a. Bright field image.

b. Convergent beam diffraction pattern from grain A, <0 0 1> zone axis.

c. CBDP from grain B, <0 0 1> zone axis.

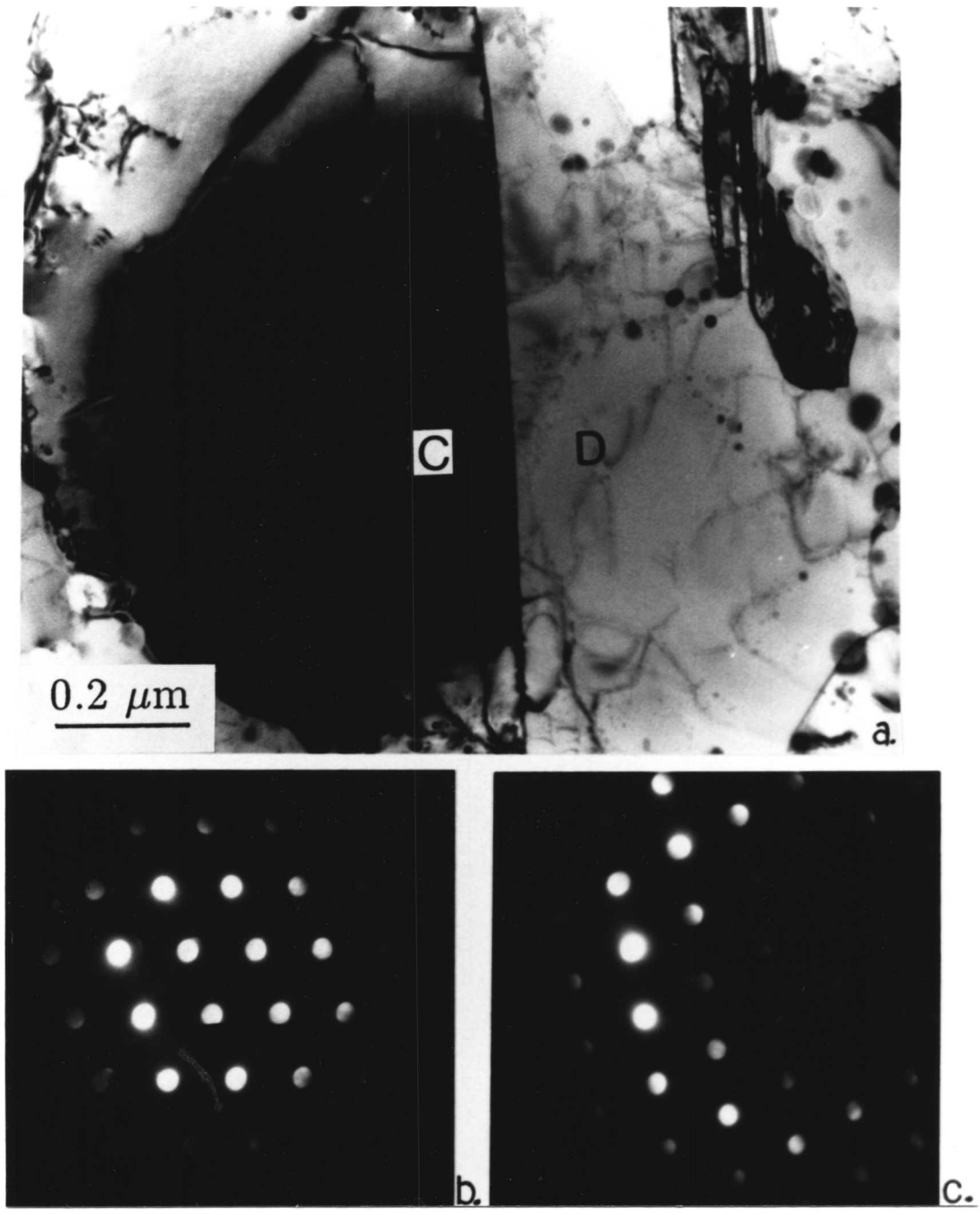

Figure 4.5. Electron micrograph and corresponding diffraction patterns from a pair of adjacent grains C and D. The axis-angle pair relating to these grains can also be represented equivalently by a rotation of 180° around <0.372 0.656 0.656> and this is near a Σ9 orientation relationship.

a. Bright field image

b. CBDP from gain C, <0 1 1> zone axis.

c. CBDP from grain D, <0 1 1> zone axis.

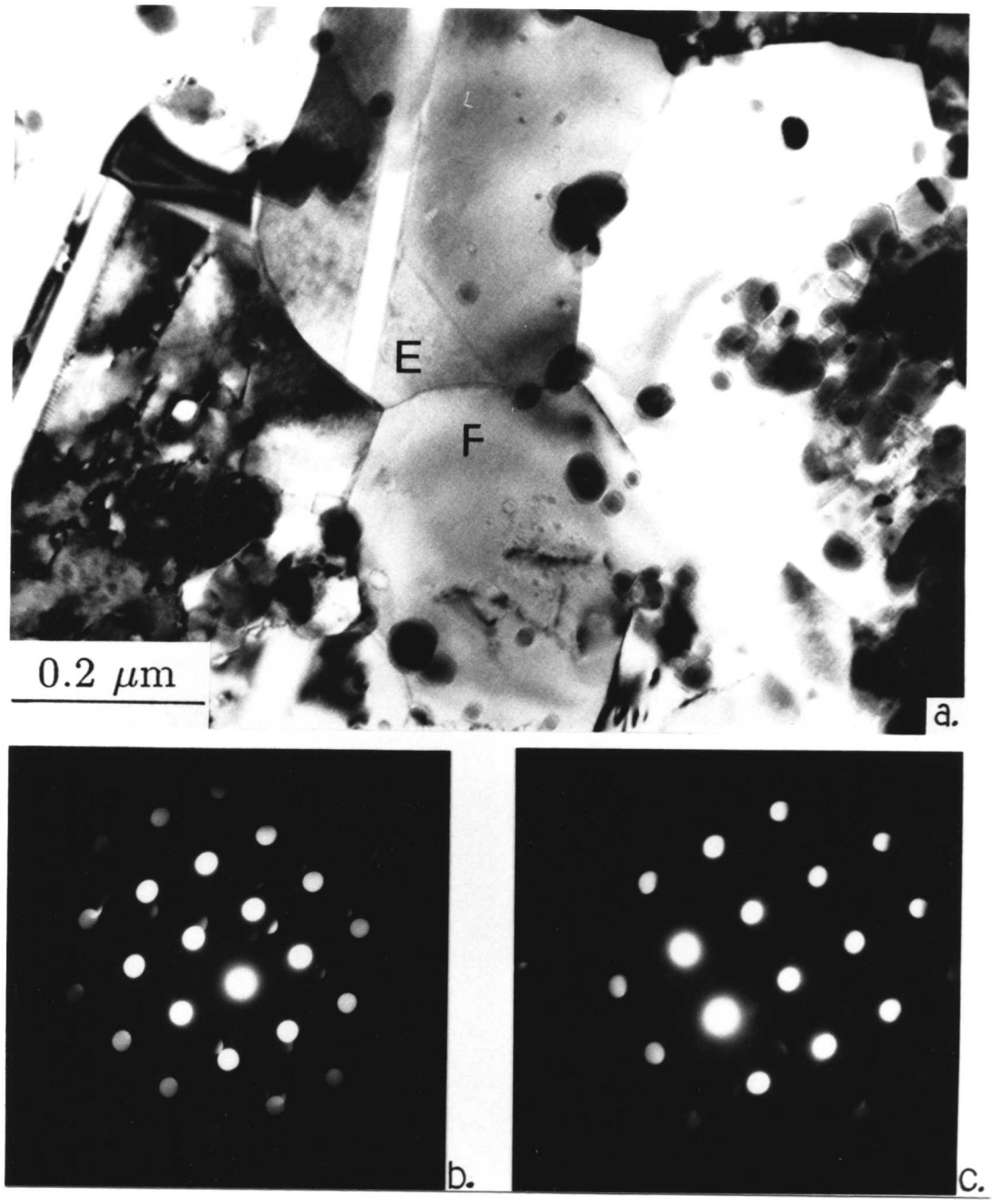

Figure 4.6. Electron micrograph and corresponding diffraction patterns from two adjacent grains E and F.

a. Bright field image.

b. CBDP from grain E, <1 1 0> zone axis.

c. CBDP from grain F, <0 0 1> zone axis.

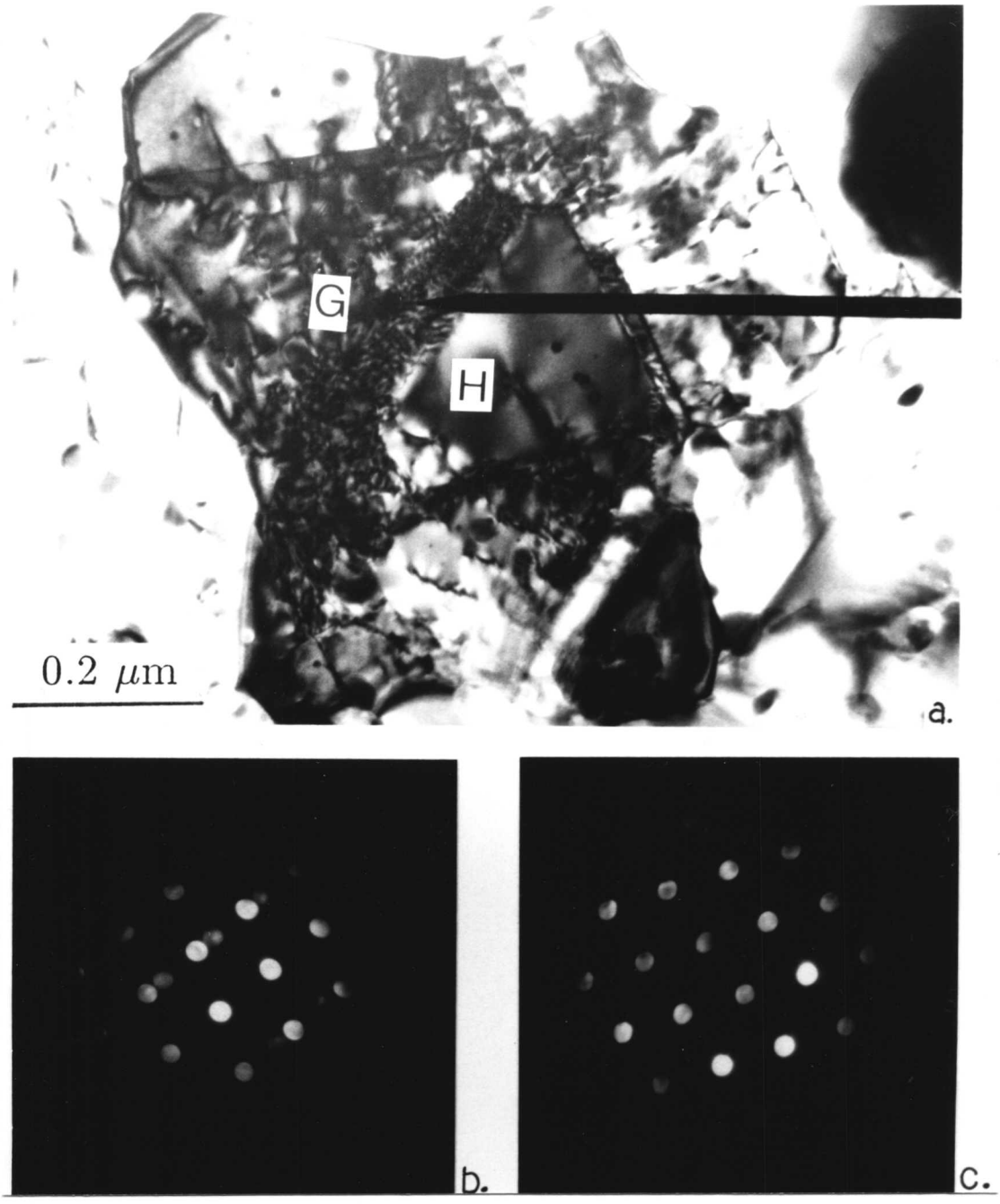

Figure 4.7. Electron micrograph and corresponding diffraction patterns from a pair of austenite grains G and H, interface boundary is defined by the arrow.

a. Bright field image.

b. CBDP from grain G, <0 0 1> zone axis.

c. CBDP from grain H, <0 0 1> zone axis.

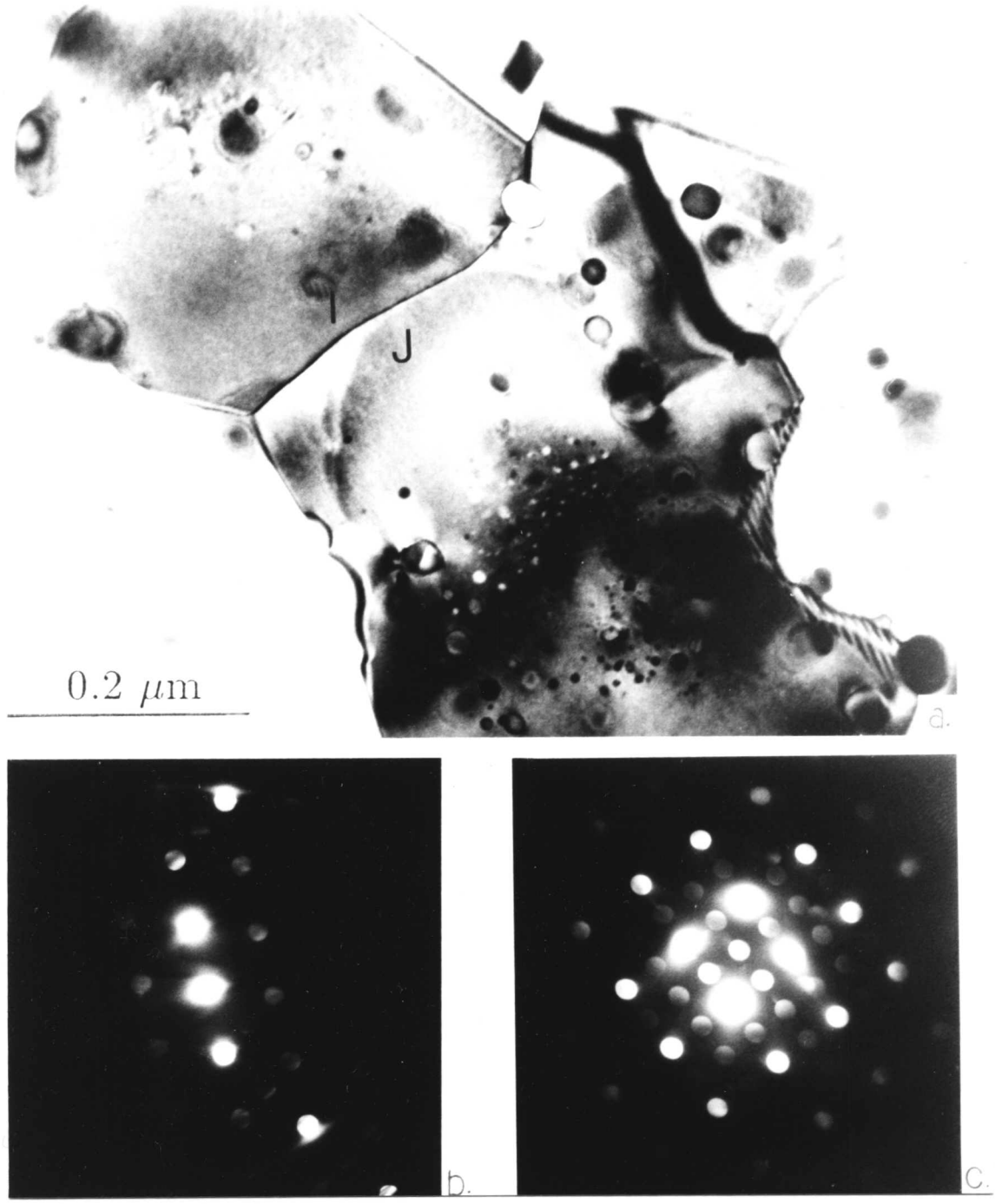

Figure 4.8. Transmission electron micrograph and corresponding diffraction patterns from two adjacent grains (I and J) of Inconel alloy MA6000 in as-received condition. The axis-angle pair relating to these grains can also be represented equivalently by a rotation of 154° around <0.650 0.322 0.687> and this is near a Σ9 orientation relationship.

a. Bright field image.

b. CBDP from grain I, <1 1 1> zone axis.

c. CBDP from grain J, <0 0 1> zone axis.

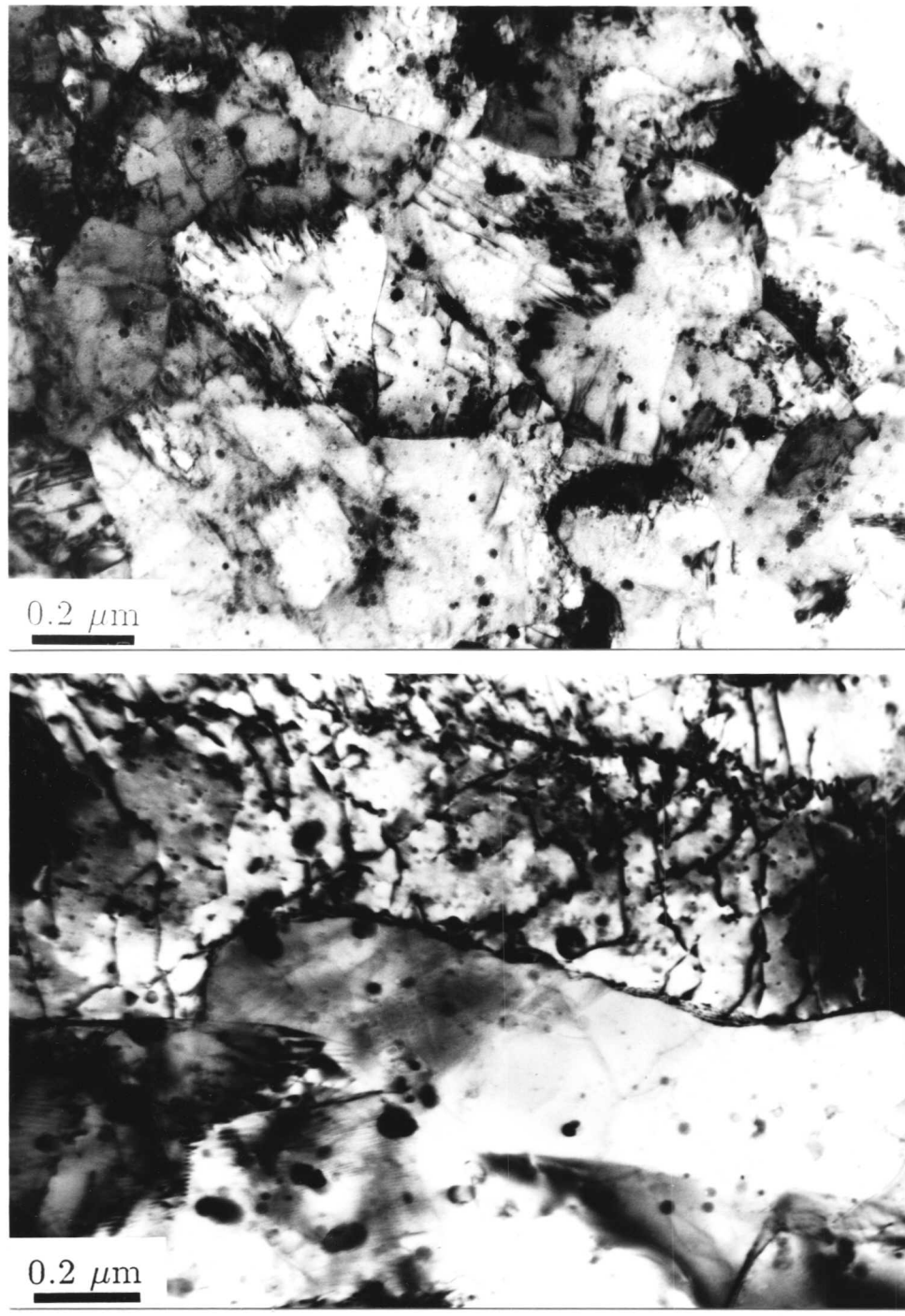

Figure 4.9. Transmission electron micrographs showing the microstructure of Incoloy alloy MA956 in as-received condition.

a. Micrograph recorded from the thin foil prepared from the transverse section of the hot-rolled bar, showing equiaxed grain structure with relatively higher dislocation density.

b. Micrograph recorded from the thin foil prepared from the longitudinal (parallel to the rolling direction) section, illustrating tangled dislocation network.

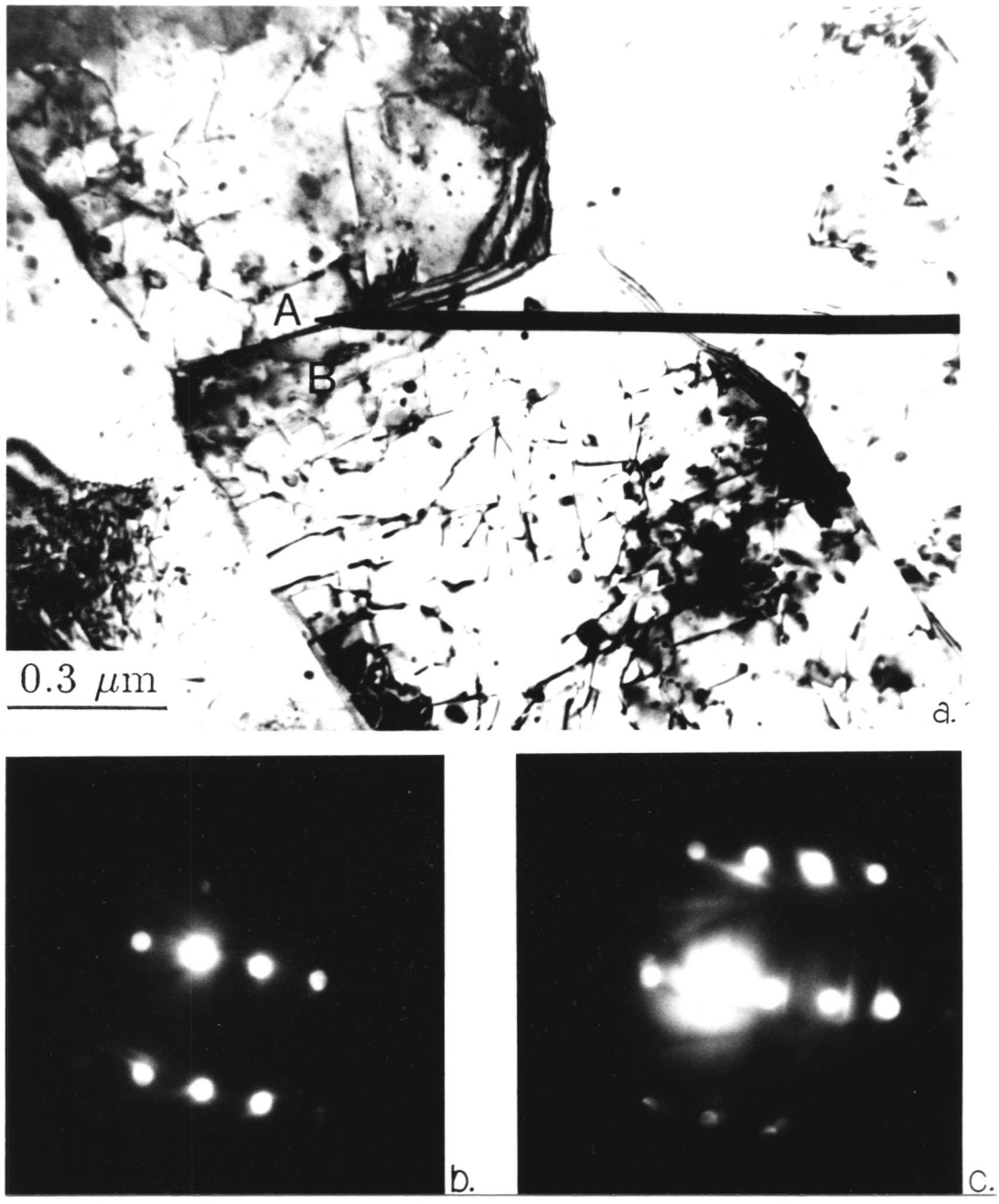

Figure 4.10. Transmission electron micrograph and corresponding diffraction patterns from a pair of ferrite grains A and B. The orientation can be represented by a rotation of 180° around <0.177 0.655 0.722> and this is near a Σ13b orientation relationship.

a. Bright field image.

b. Selected area diffraction pattern (SADP) from grain A, <1 3 3> zone axis.

c. SADP from grain B, <1 3 3> zone axis.

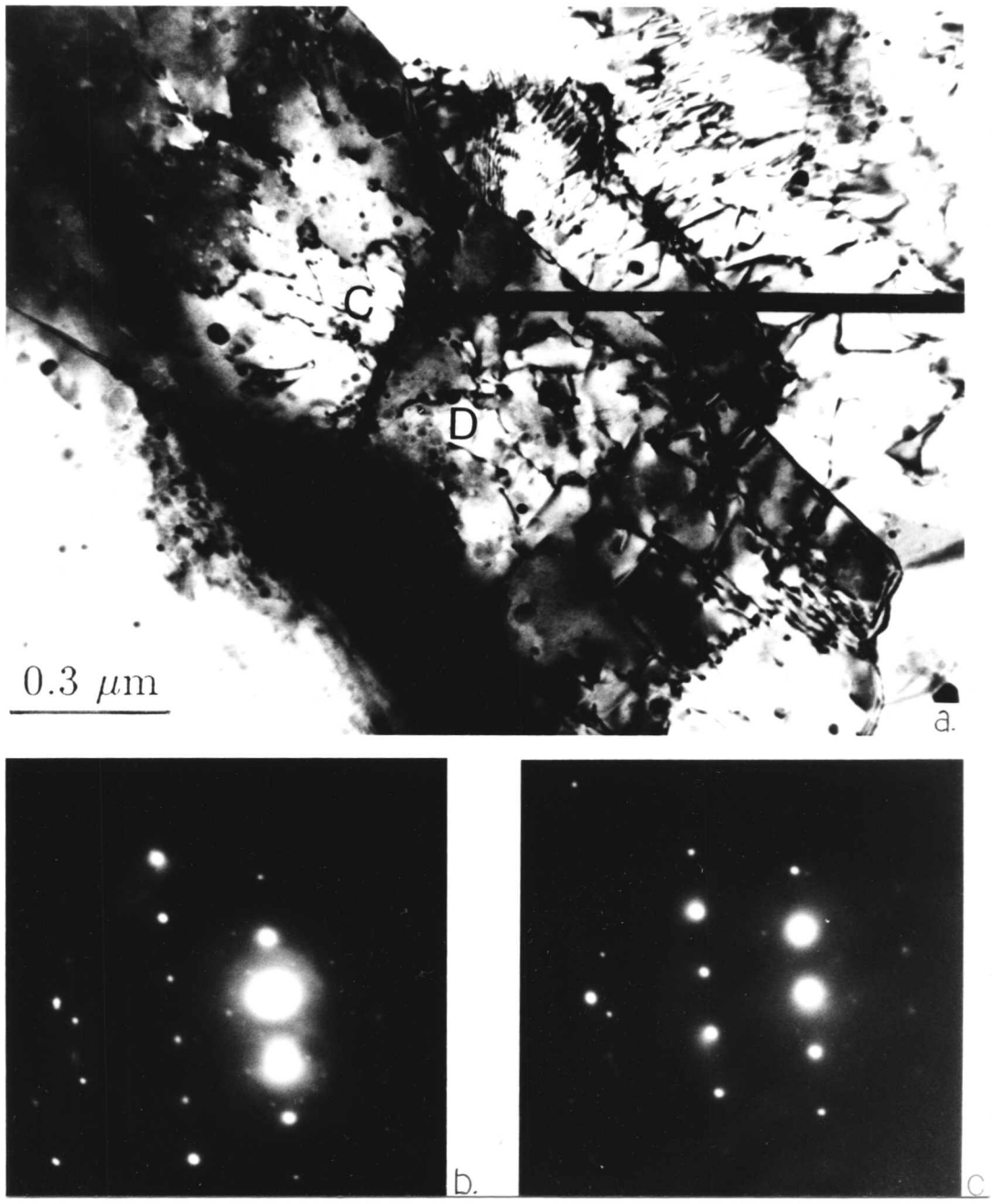

Figure 4.11. Transmission electron micrograph and corresponding diffraction patterns from a pair of adjacent grains C and D. The orientation can also be represented by a rotation of 180° around <0.205 0.814 0.542> and this is also near a Σ13b orientation relationship.

a. Bright field image.

b. SADP from grain C, <0 2 3> zone axis.

c. SADP from grain D, <0 2 3> zone axis.

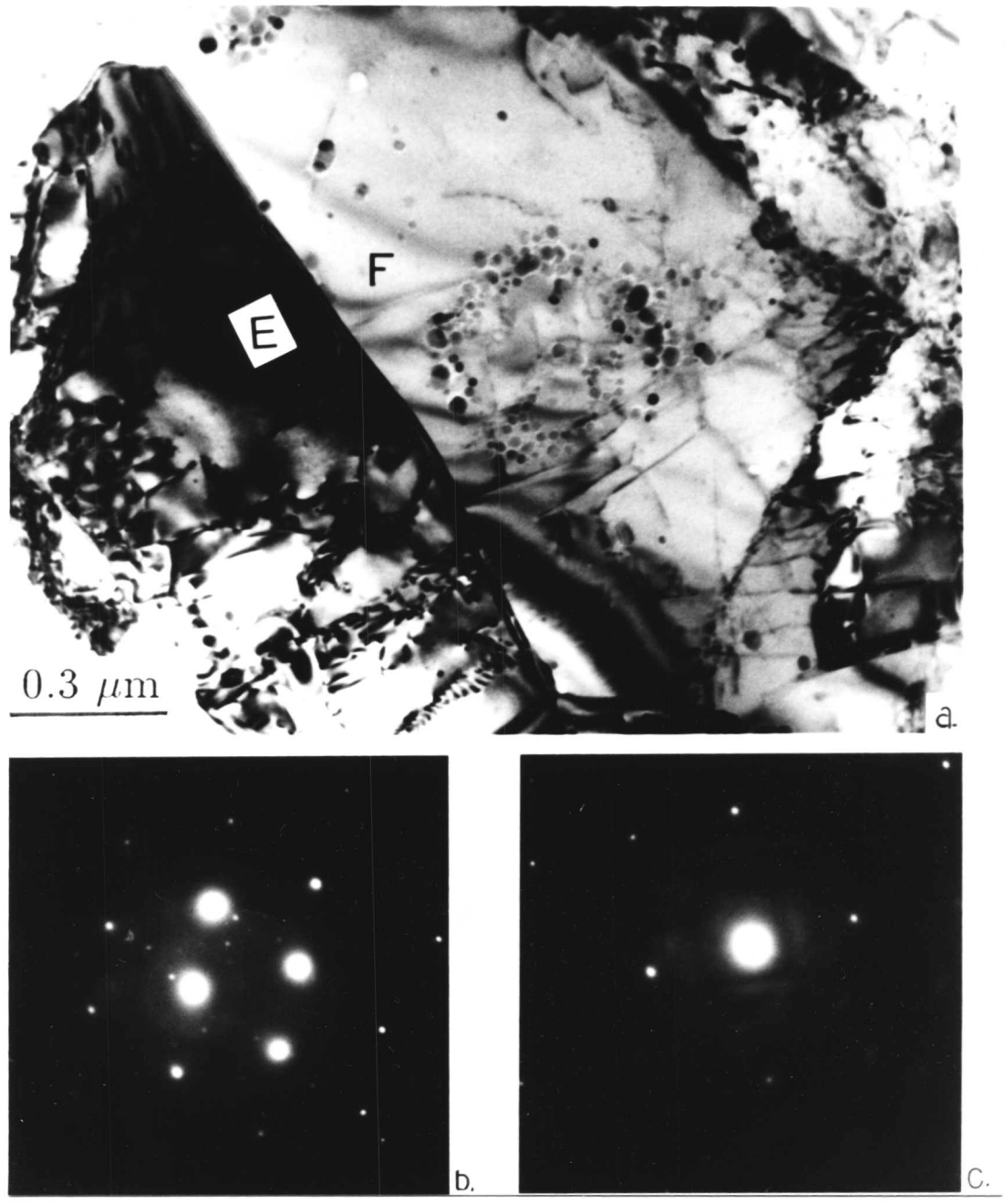

Figure 4.12. Electron micrograph and corresponding diffraction patterns from a pair of ferrite grains E and F. The orientation can be represented by <0.177 0.655 0.722>/175°, and this is near a Σ3 orientation relationship.

a. Bright field image.

b. SADP from grain E, <1 2 3> zone axis.

c. SADP from grain F, <0 1 2> zone axis.

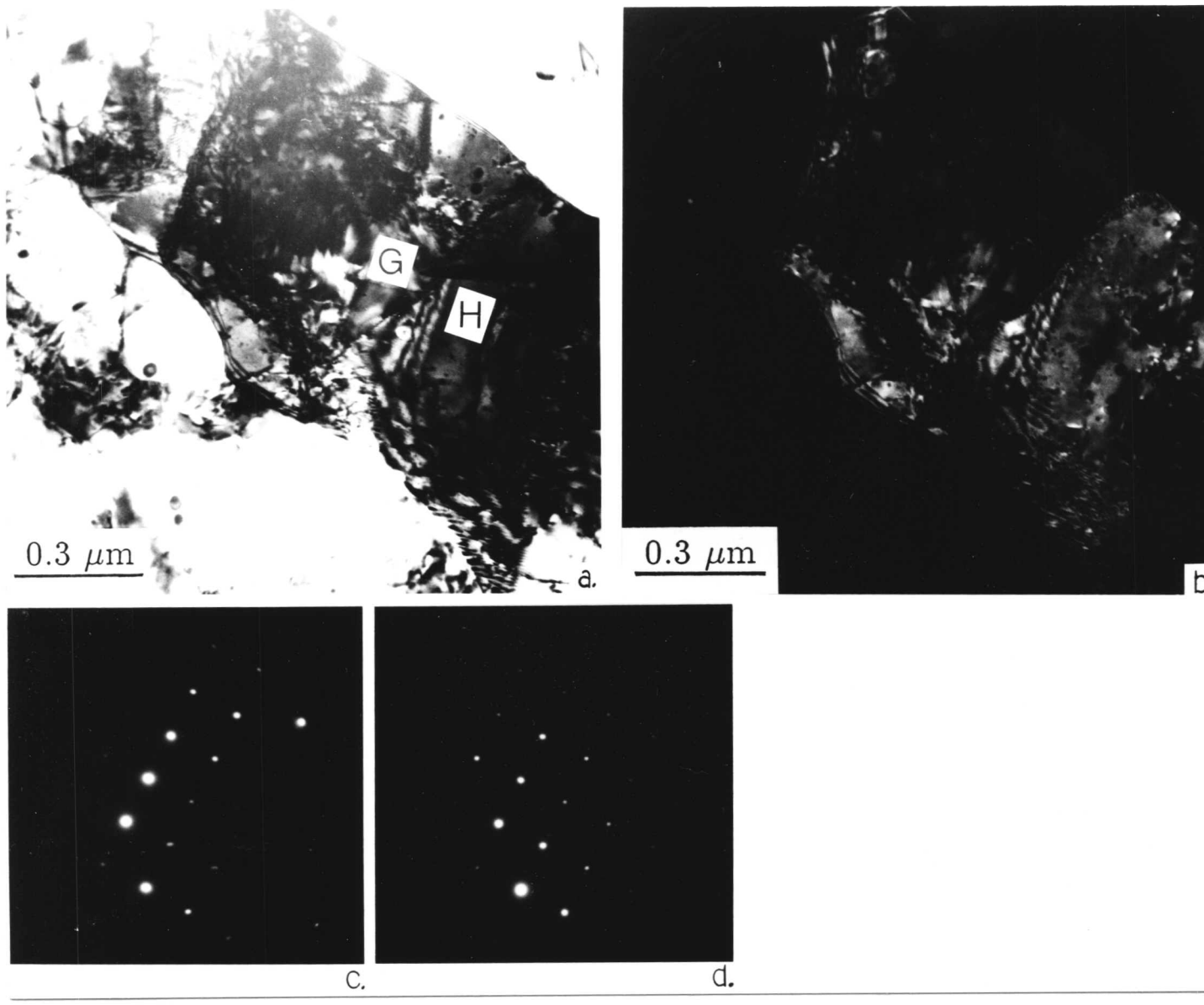

Figure 4.13. Transmission electron micrograph and corresponding diffraction patterns from two adjacent grains (G and H) of Incoloy alloy MA956 in as-received condition. The axis-angle pair relating to these grains can also be represented by a rotation of 180° around <1.000 0.008 0.000> and this is near a Σ3 orientation relationship.

a. Bright field image.

b. Dark field image of grains G and H, from the SADP shown in (c) using (2 0 0) reflection.

c. SADP from grain G, <0 0 1> zone axis.

d. SADP from grain H, <0 0 1> zone axis.

CHAPTER FIVE

Zone Annealing and Isothermal Annealing Experiments Performed on Oxide Dispersion Strengthened Nickel Base Superalloy Inconel MA6000

5.1 Introduction

There are three aspects of the microstructure of annealed ODS alloys which distinguish them from wrought or cast high-temperature alloys.

(i) a dispersion of fine oxide particles;

(ii) large elongated grains (e.g., up to several mm in length);

(iii) a strong crystallographic texture (Gessinger, 1984).

In the first part of this chapter, the topics such as alloy production, the role of alloying elements in ODS nickel base superalloys and the microstructure and properties of oxide dispersion strengthened alloys are reviewed. Attention is then turned to recrystallisation in ODS alloys and finally, the results obtained after performing zone annealing and isothermal annealing experiments to achieve directional recrystallisation in these alloys are discussed.

5.2 Alloy production

Nickel base ODS alloys are produced by an advanced powder metallurgy route called mechanical alloying (Fleetwood, 1986). The variety of powder constituents are milled together in a high energy ball mill for up to five days before being sealed in a steel can. This high energy milling causes multiple cold welding and fracturing of the powder particles, such that the final product consists of fine powder particles of uniform composition, containing the even finer dispersed, insoluble oxide particles. It should be noted that the milling is done in an inert atmosphere, which in the case of nickel base alloys is usually nitrogen. Consequently, some nitrogen is thought to become alloyed into the particles (Cairns, 1974). After consolidation by canning there is the extrusion process. For example, MA6000 is heated to 1050°C and the bar is then hot-rolled to some 90% reduction in thickness and recrystallised by zone annealing to form a coarse, highly elongated grain structure, with many of the grains extending to the length of the bar (Cairns et al., 1975). The process is

shown schematically in figure 5.1. It is the mechanisms involved in step 4 which are of main interest in the present work.

5.3 Role of Alloying Elements in ODS Ni-Base Superalloys

The functions of alloying constituents in superalloys must be understood clearly to make a judicious choice of alloy chemistry and thus optimise the properties. The role of alloying elements in Ni-base superalloys has been discussed at length in an excellent review (Jena & Chaturvedi, 1984), so that only a general outline is given here.

Superalloys are now used widely in a variety of applications at temperatures ranging from 650 to 1100°C in aggressive atmospheres, such as the combustion products of fuel and air etc. In order to function satisfactorily in such severe environments, the alloys must possess properties such as outstanding high-temperature strength, creep and fatigue resistance, excellent ductility, good impact resistance and adequate resistance to hot corrosion (Fawley, 1972).

The unique combination of properties required in these alloys is obtained by having face-centred cubic (f.c.c) matrix which is hardened by solutes and coarsening resistant precipitates. The precipitates in nickel base superalloys are primarily of the Ni_3(Al Ti Nb) type intermetallic compounds and carbides and are of a suitable structure, shape, size and distribution so as to give the desired properties and to resist microstructural changes during high-temperature service (Jena & Chaturvedi, 1984).

Chromium is used to develop corrosion resistance; aluminium, titanium and niobium promote the formation of strengthening precipitates such as γ'-Ni_3(Al,Ti), Ni_3Ti and Ni_3Nb, while elements such as molybdenum, chromium, cobalt and iron partition mostly to the γ-matrix and may increase its strength by solution hardening. They may also change the lattice parameter of the γ-phase and thereby effect coherency between γ and γ', which is an important factor influencing strength. Elements such as aluminium, titanium, niobium, tantalum, and vanadium partition mostly to γ' and therefore also influence the γ - γ' mismatch and the hardness of the γ'. Tungsten may partition either into the γ or γ' depending on the alloy composition. Several of these elements also form carbides, which may add to overall strength of the alloy. Titanium, tantalum, zirconium and niobium form primary MC carbides, while secondary carbides such as $Cr_{23}C_6$(Mo,W,Nb)$_6$C and Cr_7C_3 may form during cooling or during subsequent heat treatment or service exposure (Holt & Wallace, 1976).

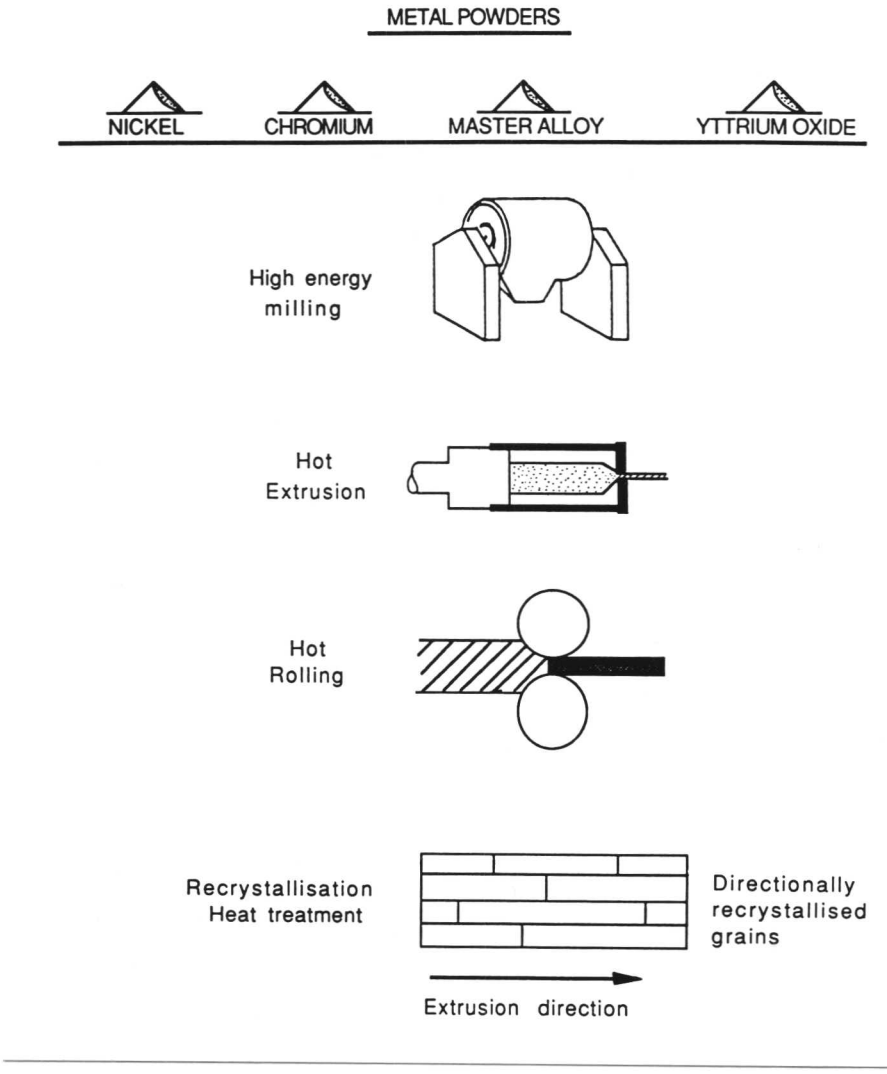

Figure 5.1. Schematic drawing of the processes involved in mechanical alloying (after, Incomap data sheet for ODS MA6000).

5.4 Microstructure and Properties of ODS Alloys

The ODS alloys which have been investigated for the work described in this thesis are, i) Ni-Cr and ii) Fe-Cr base, and their chemical compositions are given in Table 3.1 (see chapter 3). The alloys were manufactured by Wiggin Alloys Ltd. (Hereford); which is part of the INCO group of companies. This section is concerned mainly with the microstructure, properties and applications of ODS Ni-base superalloy MA6000.

The microstructure of MA6000 before the final recrystallisation heat treatment shows a very fine grained structure of the extruded and hot-rolled material, with an incredibly fine grain size of typically 0.2μm diameter (Hotzler & Glasgow, 1980).

Until recently, the Y_2O_3 particles have generally been considered to be insoluble and not to react with the matrix. However, a recent X-ray diffraction study of the oxide dispersion after alloy processing showed them to be a mixture of yttria and yttrium aluminates (Erdos, 1983) indicating some reaction with the metal matrix.

In addition to the fine (10-30nm) yttria-base particles, the coarser (0.5-4μm) second-phase particles have also been reported (Hotzler & Glasgow, 1980, and Gessinger, 1984) and the maximum size for inclusion is reported to be in the range of 50 to 70μm by Hoffelner and Singer (1985). These larger particles are strongly aligned in the extrusion direction and appear as stringers in the final recrystallised alloy. They have been identified as a mixture of titanium carbo-nitrides Ti(C,N), and aluminium oxide (Al_2O_3) and are assumed to have resulted from nitrogen and oxygen being included in the powder during milling and combining with the titanium and aluminium in the alloy (Cairns et al., 1975). It has also been suggested by Cairns et al., that it is the stringers of coarser particles that impede lateral grain growth. The massive elongated grains show a strong <110> texture parallel to the working direction for the γ' strengthened, nickel base superalloy MA6000 (Howson et al., 1980).

ODS nickel base superalloys are suited mainly for high-temperature and long service time applications involving operation at comparatively low stress levels (Gessinger, 1984) with both the dispersoids and the large grain aspect ratio contributing to the high creep strength exhibited by the alloys (Hoffelner & Singer, 1985).

At intermediate temperatures, MA6000 has a stress rupture strength that is equal to that attained by most conventional nickel base superalloys, while at elevated temperatures the stress rupture strength of MA6000 is superior to all other ODS materials (Howson et al., 1980). As for as

maintaining strength at high temperatures in the face environmental attack is concerned, MA6000 is less reliant on coatings than other alloys, and has a very good cyclic oxidation resistance. It seems particularly suited to small blades operated uncooled at high temperatures (Fleetwood, 1986).

5.5 Recrystallisation in Oxide-Dispersion-Strengthened Alloys

An important factor which gives ODS alloys their good creep strength is their massive elongated grain morphology and it is crucial that this morphology is produced throughout the material (Wilcox & Clauer, 1972, Artz & Singer, 1984). After powder consolidation and extrusion, the material is fine-grained and a high temperature anneal is required to bring about the required grain growth. It is the mechanism of this change, from grains less than 0.5μm in size to ones that often exceed 1mm in length, that has still to be understood. The process of grain growth in ODS nickel base superalloys has generally been regarded as being similar to that of secondary recrystallisation or abnormal grain growth with the implication that the major driving force is the reduction in grain boundary area (Gessinger, 1984).

In order to explain this phenomenon, the mechanism behind the bulk recrystallisation of ODS alloys needs to be fully understood. Crucial to that mechanism is the condition of the fine-grained alloy and the energy stored in it as a result of its thermomechanical processing. This section discusses the present level of knowledge about the recrystallisation characteristics of ODS alloys, including the effect of hot working on the recrystallisation of ODS alloys.

In order to avoid confusion, it is important at this stage to define some of the terminology used in describing the condition of the alloys. Much of the literature refers to the alloy as being in either the unrecrystallised or recrystallised condition. The use of term "unrecrystallised" refers to the as-consolidated or deformed material and the fact that it is in the fine-grained condition, and has yet to undergo the high temperature heat treatment. Nothing should be inferred about the stored energy in the alloy or its dislocation density. The term "recrystallised" is used to refer to the coarse-grained metal after high-temperature annealing.

5.5.1 The As-Deformed Oxide Dispersion Strengthened Alloy

If the observed formation of highly elongated grains is purely a secondary recrystallisation phenomenon then, prior to the high-temperature heat treatment, the fine-grained material must have already undergone primary recrystallisation, i.e., the grain structure is already equiaxed, strain free and with a low dislocation density. Since the powder, prior to consolidation, has a very high

dislocation density due to mechanical alloying process (Fleetwood, 1986), the recovery and primary recrystallisation process would have had to occur during consolidation i.e., dynamic recrystallisation. This opinion that the as-consolidated material has undergone complete primary recrystallisation has been held by many workers (e.g., Cairns, 1974, Hotzler & Glasgow, 1982), whose transmission electron microscopic studies have shown an average dislocation density of around $10^{13}m^{-2}$ in as-consolidated ODS alloy MA6000. It has also been reported in number of studies that the microstructure is not completely uniform (Cairns et al., 1975, Singer and Gessinger, 1982); a few of the grains in the samples examined in that study were found to be elongated.

This suggests that the alloy is only partially recrystallised in the fine-grained condition and led Singer and Gessinger (1982) to suggest that during the consolidation process the alloy can undergo superplastic deformation. Singer and Gessinger (1981) have also shown that as-consolidated MA6000 can be subsequently superplastically deformed. Superplastic deformation could certainly be used to explain some of the features described above. During superplastic deforming, groups of grains slide over each other until an unfavourably oriented grain obstructs the process. The resultant stress concentration is relieved by slip within the blocking grain (Edington et al., 1976). This will give rise to the occasional heavily dislocated and elongated grains seen in the as-consolidated material.

It is clear from the above discussion that the condition of the fine-grained as-extruded alloy is far from being simply primarily recrystallised. The variation of microstructure reported, suggests that the amount of dynamic recrystallisation and superplastic deformation varies depending upon grain size, alloy composition and processing conditions. The energy content of different batches of same alloy may vary greatly, which means that their response to recrystallisation will tend to be different.

It is thought that the recrystallisation response of MA6000 is less sensitive to its thermomechanical history than any other ODS nickel base superalloy (Gessinger, 1984).

5.5.2 General Features of Secondary Recrystallisation in ODS Alloys

There have been a number of studies designed to arrive at the optimum grain structure in the ODS alloys. Most of the recrystallisation characteristics in ODS alloys are still not fully understood which, perhaps, is not too surprising since the mechanism of secondary recrystallisation in simpler systems is still unclear (Cahn, 1983).

The general features of the secondary recrystallisation in ODS superalloys are described below:

(a) There is a well defined minimum temperature at which abnormal grain growth will occur and this is called the secondary recrystallisation temperature.

(b) The grain coarsening associated with secondary recrystallisation process is very rapid. Once above the recrystallisation temperature, it may take only 5 minutes for complete secondary recrystallisation (Cairns et al., 1975).

(c) The recrystallised grain structure is sensitive to heating rate and temperature gradient.

(d) Grain size and grain aspect ratio (GAR) are increased by zone annealing (Cairns et al., 1975).

(e) Grain growth results in a characteristic texture (Claudia et al., 1979).

(f) Twinning may occur in the recrystallised grains.

(g) Annealing just below the recrystallisation temperature causes uniform growth of primary grains and subsequent high-temperature annealing is unable to cause further grain growth. This has led to the idea of the minimum heating rate to achieve recrystallisation (Cairns et al., 1975).

(h) Prestraining can suppress the grain growth during secondary recrystallisation (Singer & Gessinger, 1982).

5.5.3 Role of Gamma Prime Precipitate during Grain Growth in Alloy MA6000

The recrystallisation characteristics of the γ' strengthened alloy MA6000 differ in some respects from the other nickel base alloys which do not contain any γ' precipitates. The γ' solvus in MA6000 has been measured at between 1160 and 1180°C and the dissolution of the γ' has been thought to be the trigger for secondary recrystallisation (Hotzler & Glasgow, 1980, Mino et al., 1984). Most of the work on the recrystallisation of ODS alloys then goes on to conveniently ignore the γ'-free alloys when explaining the secondary recrystallisation mechanism.

The observations reported by Hotzler and Glasgow (1980), and Mino et al., (1984) suggest that γ' dissolution is, in fact, a "red herring" in ODS alloy recrystallisation. If γ' dissolution is the trigger, then the secondary recrystallisation temperature for any alloy would vary with the γ' solvus. However, there is no evidence to support this. MA6000, with 50-55 vol% of γ' (Gessinger, 1984) recrystallises at a very similar temperature to the γ'-free MA754 (Markham, 1988). Admittedly the transformation temperature is much better defined in MA6000 but this could be explained by the

difference in the stored energy of the two alloys. A study by Dahlen & Winberg (1979), of recrystallisation in a γ' containing dispersion free alloy showed that it was the migrating grain boundaries that caused the γ' precipitate to dissolve and reprecipitate again in the recrystallised grain.

5.6 Material

To study the directional recrystallisation, zone annealing and isothermal annealing experiments have been performed on MA6000 supplied in the as-deformed condition in the form of 20mm diameter bar hot rolled from 1040°C in one heat, from starting size of 54mm diameter bar to a finish size of 25mm diameter bar (an 54% reduction).

To obtain a directionally recrystallised grain structure, one batch of samples was cut into rectangular rods with dimensions of 4 x 4 x 20mm, the length being parallel to the rolling direction. The second batch of samples was prepared with the length lying perpendicular to the rolling direction. The samples were zone annealed using a crystal grower. A schematic diagram of the crystal grower adopted and used for zone annealing is shown in figure 3.2 of chapter 3.

The experiments were performed at four different peak temperatures ranging from 1100 to 1300°C, with range of specimen travel speeds (0.4, 0.8, 1.4 3.2, 5.0, 7.7 and 10.0 mm/min) for each temperature.

Optical and transmission electron microscopy was conducted on longitudinal sections since the elongated grain microstructure can only be observed on sections. The various directions are illustrated as a sketch (figure 5.2), to avoid any confusion.

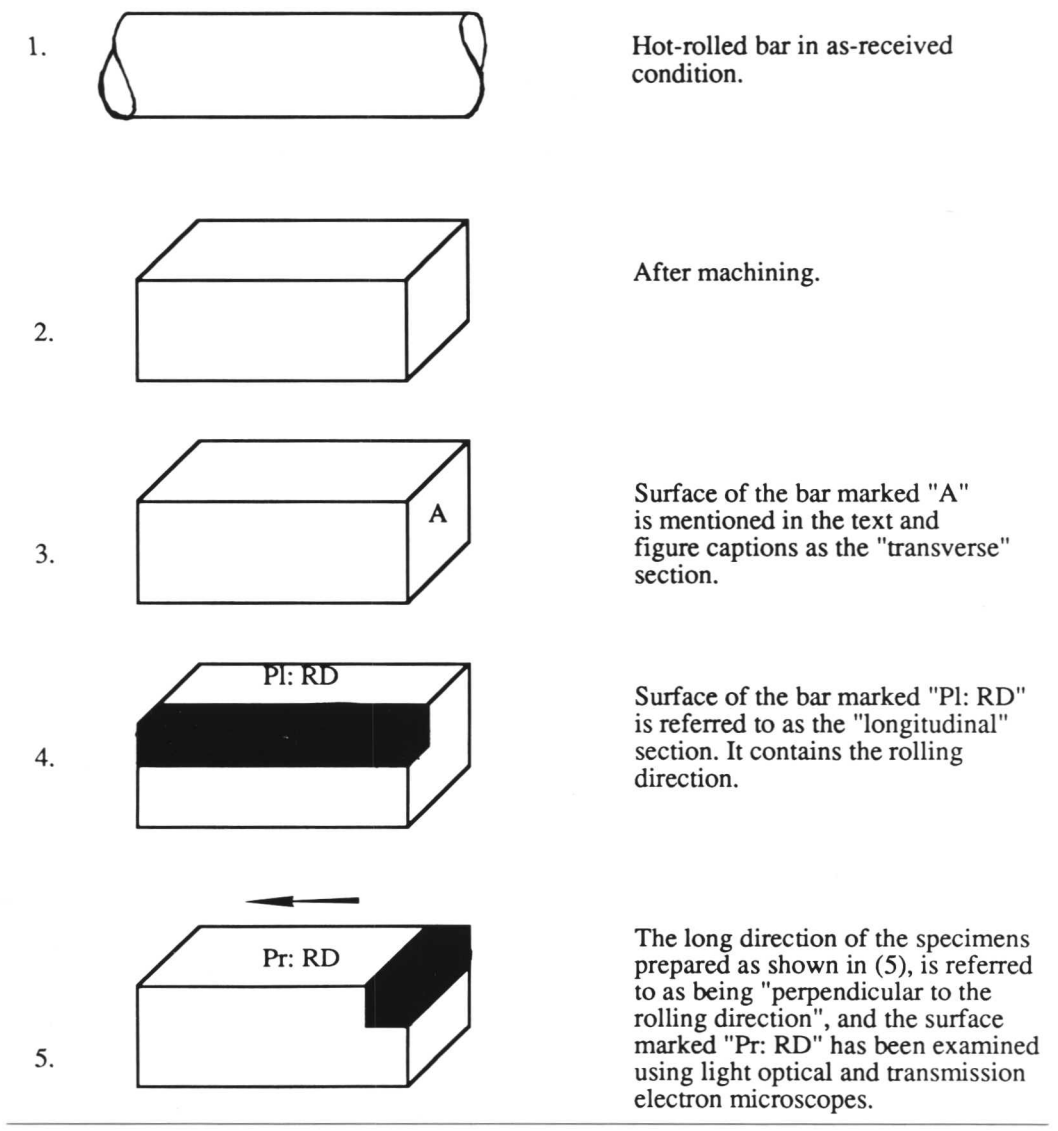

Figure 5.2. Sketch illustrating the planes examined by light optical and transmission electron microscopy. The arrow indicates the rolling direction, and the each specimen travelled through the zone annealing furnace in a direction parallel to its longest dimension.

5.7 Results

The results obtained in the form of microstructure and hardness tests, after zone annealing Inconel alloy MA6000, are listed in Tables 5.1a, b and c. From Table 5.1a, and figure 5.5, it can be seen that when the peak temperature is T_p = 1100°C, during zone annealing, alloy MA6000 is hardly altered in microstructure and hardness.

Further zone annealing experiments have also been done with T_p = 1150°C, in which the temperature was monitored at three points on the specimen at (9mm from each end and along the centre of the specimen length) in order to highlight any variation in thermal cycles as a function of position along the samples. The diagram associated with Table 5.2 illustrates the location of the thermocouples. The measurements indicate that with a specimen travel speed of 1.4 mm/min, all positions along the sample experience about the same peak temperature (T_p). However, as the speed is increased to (3.2 or 5.0 mm/min), T_p is found to vary by about 50°C along the length of the specimen, its value increasing as function of distance from the entry end of the sample. This is expected since regions entering the R. F. coil at later times will also receive a flux of heat from the parts of the sample which have already passed through the coil, and hence will be able to achieve higher peak temperatures, which is consistent with the experimental results. This effect should increase in significance as the specimen travel speed increases since temperature gradient also increase with the speed.

According to Hotzler and Glasgow (1980), the transformation in MA6000 from fine grains (wrought type of grain structure) to coarse columnar grains occurs upon heating the material above the γ' solvus temperature i.e., 1165°C, when the samples are annealed in a temperature gradient. Figure 5.6 shows the microstructure of a longitudinal section (containing the rolling direction) after zone annealing with T_p = 1160°C, for different specimen travel speeds. The start of the zone anneal is on the left hand side of the micrographs, and the columnar grains have grown from the left to the right side. The microstructural results shown in figure 5.6, are in good agreement with the above statement given by Hotzler and Glasgow (1980).

Transmission electron micrographs (figure 5.7a & b) recorded from thin foil samples prepared parallel to the longitudinal section of the samples zone annealed at T_p = 1160°C (travel speed of 5 mm/min), revealed a random distribution of fine and coarse particles in the matrix. In the recrystallised samples, grain boundaries were extremely rare in thin foil samples due to the small size of the region examined when compared with the coarse grain structure, but after considerable

effort some boundaries were observed, but no alignment of particles was detected on or along the grain boundaries. Further examination of the thin foils from the same zone annealed sample T_p = 1160°C, 5 mm/min), revealed a considerably higher density of annealing twins and dendritic shaped γ' precipitates (figures 5.8 - 9).

In many specimens, regions of equiaxed grains could be observed at both ends of the specimens (figure 5.6c). This is believed to be a consequence of enhanced "nucleation" of secondary recrystallisation at the end surfaces, since the R.F. source heats the surface of the sample.

The following notation is used to indicate the microstructure and processing in the tables used to summarise the experimental data:

Symbols	Terms
D	As-deformed
DX	Directionally recrystallised
HV	Vickers hardness
PDX	Partial directionally recrystallised
Pl: RD	Zone annealed parallel to the rolling direction
Pr: RD	Zone annealed perpendicular to the rolling direction
PX	Partially recrystallised
T_p	Peak temperature
X	Recrystallised with an equiaxed grain microstructure

Table 5.1a. Microstructure and Vickers hardness data obtained for Inconel alloy MA6000, after zone ann
and specimen travel speeds. Hardness in the as-received condition was 645 HVN(10kg).

T_P °C	Specimen	Specimen Travel Speed mm/min						Hardness Vickers HVN(10kg)					
	Condition	0.8	1.4	3.2	5.0	7.7	10.0	0.8	1.4	3.2	5.0	7.7	10.0
1100	Pl: RD	D	D	D	D			599	620	642	634		
								620	613	634	634		
								642	627	642	642		
								620	627	634	642		
								592	634	634	642		
1100	Pr: RD	D	D	D	D			606	627	642	642		
								613	627	642	642		
								627	634	634	649		
								627	627	642	642		
								613	642	642	642		
1160	Pl: RD	DX	DX	DX	X	X	X	493	514	525	525	519	536
								498	498	525	530	536	530
								503	493	514	508	530	536
								498	498	508	519	530	530
								488	493	514	519	519	536

Table 5.1b. Microstructure and Vickers hardness data obtained for Inconel alloy MA6000, after zone annealing a
travel speeds.

T_P °C	Specimen	Specimen Travel speed mm/min							Hardness Vickers HVN(10kg)						
	Condition	0.4	0.8	1.4	3.2	5.0	7.7	10.0	0.4	0.8	1.4	3.2	5.0	7.7	10.0
1200	Pl: RD	DX	DX	DX	DX	DX	PDX	PX	483	478	478	473	493	519	525
									488	488	495	488	488	525	525
									478	495	455	508	473	525	519
									478	493	495	493	478	530	542
									468	488	488	488	498	519	530
1200	Pr: RD				DX	PDX	X					498	519	508	
												514	536	525	
												508	542	542	
												525	525	542	
												498	493	548	

Table 5.1c. Microstructure and Vickers hardness data obtained for Inconel alloy MA6000, after zone-annealin travel speeds.

T_P °C	Specimen Condition	Specimen Travel Speed mm/min						Hardness Vickers HVN(10kg)						Mea
		0.8	1.4	3.2	5.0	7.7	10.0	0.8	1.4	3.2	5.0	7.7	10.0	0.8
1300	PI: RD	DX	DX	DX	DX	PDX	X	413	421	437	468	483	503	420
								413	433	446	488	508	503	
								446	464	503	503	514	542	
								413	446	503	503	508	519	
								413	433	455	483	483	493	
1300	Pr: RD		DX	PDX	X				493	498	519			
									478	519	525			
									493	519	536			
									473	498	503			
									473	483	483			

Table 5.2. Temperatures recorded at three positions on the same sample during zone annealing at T_p = 1150°C. Note that the travel time through the R. F. coil increases with the row number in each tabulation.

Specimen Travel Speed, 1.4 mm/min

Point 1	Point 2	Point 3	
1135	1025	870	
1140	1050	890	Peak temperature measured at point 1
1080	1113	970	
1025	1130	1020	Peak temperature measured at point 2
890	1065	1130	
860	1033	1143	Peak temperature measured at point 3

Specimen travel speed, 3.2 mm/min

Point 1	Point 2	Point 3	
1110	1020	855	Peak temperature measured at point 1
990	1125	1030	Peak temperature measured at point 2
860	1030	1145	Peak temperature measured at point 3

Specimen travel speed, 5.0 mm/min

Point 1	Point 2	Point 3	
1076	1025	865	Peak temperature measured at point 1
975	1112	1040	Peak temperature measured at point 2
848	1012	1148	Peak temperature measured at point 3

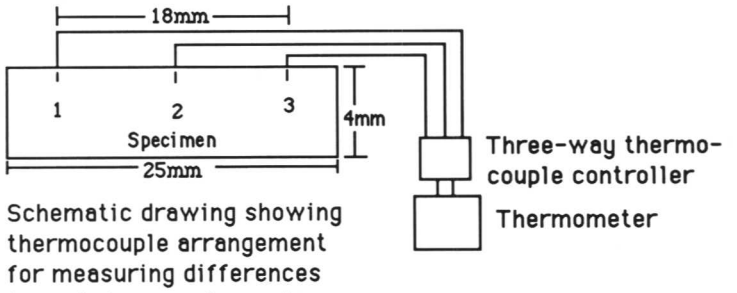

Schematic drawing showing thermocouple arrangement for measuring differences in peak-temperature, at different parts of the specimen during operation.

Figure 5.11 shows the microstructure obtained after zone annealing samples at T_p = 1300°C. Extremely coarse grained regions are observed at the specimen ends, the coarseness of these grains decreasing as the specimen travel speed increases. These end effects are, as mentioned earlier, a consequence of the R. F. heating technique. The free surfaces at the ends of the samples are susceptible to R. F. heating effects, giving relatively lower temperature gradients and hence inducing equiaxed grain growth. The influence of the end surfaces would be expected to be reduced as the speed increases, and hence, a lower grain size is seen at the ends of the specimen travelled at higher speeds.

5.7.1 Particle Alignment

An attempt was also made to investigate any tendency for the alignment of oxide particles along the extrusion direction, since such alignment could potentially lead to anisotropic grain growth of the type observed. Figure 5.12, which is taken from a polished but unetched specimen of MA6000 in the as-received condition, shows that there are some coarse particles aligned along the working direction. These are not polishing artefacts because the features appeared even when the samples were prepared with the grinding and polishing directions normal to the working direction (figure 5.12b, is such a case).

Note that most of the yttria particles are supposed to be very small (20-40 nm), so that those apparent in figure 5.12 must represent the very much coarser part of the size distribution. Transmission electron microscopic studies, attempted to investigate the effect of fine particles, failed to reveal any obvious alignment of those particles in the alloy.

To see whether the observed degree of particle alignment is significant with respect to recrystallisation behaviour, zone annealing experiments were performed on specimens prepared with their long axes perpendicular to the rolling direction. The recrystallised microstructures recorded after zone annealing these specimens at peak temperatures of 1200 and 1300°C, perpendicular to the rolling direction, at specimen travel speeds 1.4, 3.2 and 5.0 mm/min, are shown in figures 5.13 and 5.14. Although there is clearly some tendency towards directional recrystallisation, but there exist large regions of equiaxed grain structure . Furthermore, even the mildly directional grains are not as anisotropic as those observed on zone annealing under identical conditions but with the travel direction parallel to the rolling direction (see figure 5.10 & 5.11). These results indicate that there is indeed an influence of particle alignment in promoting directional recrystallisation with high growth

rates along the working direction, but as will be seen later, the effect for MA6000 is far smaller than for the ODS steels to be discussed in chapters 6 and 7. Also, to obtain a highly directional microstructure in MA6000, it is clearly necessary to anneal in a thermal gradient, at suitable temperatures, specimen travel speeds, and along specific directions.

An enormous difference in grain size can be seen from the micrographs shown in figures 5.10 and 5.11. These differences are consistent with the hardness data listed in Table 5.1b & c, which clearly show that the decrease in grain size correlates with an increase in the hardness.

Quantitative grain size measurements were carried out using the mean linear intercept method on micrographs taken from longitudinal sections of the samples. It turns out that the accurate measurement of grain size is very difficult because of difficulties experienced in clearly identifying the grain boundaries. Approximate grain size measurements from fully recrystallised specimens are listed in Table 5.3.

Table 5.3. Grain size as-measured by the linear intercept method, after zone annealing Inconel alloy MA6000 at different temperatures and specimen travel speeds. The quantities given in brackets indicate the standard deviations of the measurements.

Material	T_p	Specimen Travel Speed mm/min						
	°C	0.4	0.8	1.4	3.2	5.0	7.7	10.0
		Grain Size (G') mm						
MA6000	1160		0.17	0.17	0.16	0.12	0.13	0.09
			(0.07)	(0.06)	(0.07)	(0.06)	(0.04)	(0.04)
	1200	0.26	0.19	0.23	0.15	0.10	0.13	0.11
		(0.06)	(0.07)	(0.06)	(0.04)	(0.04)	(0.04)	(0.04)
	1300		0.19	0.20	0.14	0.12	0.09	0.10
			(0.07)	(0.07)	(0.06)	(0.06)	(0.07)	(0.04)

The grain size measurements were done for two reasons, a) to measure the width of the columnar grains after each successful directional recrystallisation experiment, b) to interpret the data obtained from the hardness tests.

It can be seen from Table 5.3, that the grain size measured from the specimen zone annealed at T_p = 1200°C and a specimen travel speed of 0.8 mm/min is relatively low and its hardness is relatively high (500 HV). But as the speed was increased the grain size also increased, but eventually it decreased again, such a peak in grain size is difficult to explain.

The temperature versus time data recorded during zone annealing together with a corresponding set of data for exp(-Q/RT) as a function of time are illustrated in figures 5.3 and 4 respectively. These latter data are henceforth referred to as the "kinetic strength" data. The concept of the "kinetic strength" of an anisothermal heat treatment is discussed and mathematically expressed in chapter six.

As recrystallisation involves the movement of grain boundaries, it is appropriate to consider the transfer of atoms across the boundary as it moves, as a rate limiting step in the process. The activation energy Q for this process will depend on the coherency of the boundary. For a coherent boundary Q should be similar to that for volume diffusion. For an incoherent boundary, Q should be about half the value for self diffusion (Christian, 1965).

To calculate D from the experimental data, the value for Q has taken equal to the value for the tracer diffusion coefficient of pure nickel, which is equal to 284,716 J mol^{-1} as reported by Weast (1976-77). Since there is no transition from directionally recrystallised to partial directional recrystallisation observed at any temperature and speed used to directionally recrystallise the nickel base superalloy MA6000, so it was found difficult to measure the activation energy Q (from the experimental data), required for MA6000 to directionally recrystallise.

5.8 Summary

To obtain directional recrystallisation, zone annealing experiments were performed on oxide dispersion strengthened nickel base superalloy MA6000. Optical and transmission electron microscopy were used to analyse the microstructure in the as-received condition, which revealed that MA6000 have a very small grain size (0.17μm).

A range of peak temperatures and specimen travel speeds for zone annealing were used to investigate directional recrystallisation. Directional recrystallisation and the associated substantial decrease in hardness was only observed to occur, for the conditions studied, when the peak temperature exceeded 1100°C.

Some alignment of relatively coarse particles was found to be present in the fabricated alloy, and this seems to promote the growth of grains along the working direction during secondary

recrystallisation. The effect of particle alignment on directional recrystallisation was demonstrated by zone annealing experiments performed on samples prepared normal to the rolling direction. The resulting grain structure was less anisotropic when compared with samples zone annealed with travel direction parallel to the working direction. Transmission electron microscopy failed to reveal any obvious alignment of the very fine (20-40 nm) yttria particles in the alloy, so it is only the coarser, optically resolvable particles which are responsible for promoting anisotropic growth.

5.9 Isothermal Annealing of ODS Alloy MA6000

Isothermal annealing experiments were also performed on MA6000 using conventional resistance heating furnaces. As will be seen later, some mechanically alloyed metals tend to directionally recrystallised even during isothermal annealing.

The specimens were annealed isothermally at temperatures ranging from 1100 to 1300°C, at 100°C intervals. They were kept in the furnace for 900 seconds initially, subsequent annealing periods being doubled for each successive heat treatment, to limiting time periods of 230400, 57600 and 14400 seconds at 1100, 1200 and 1300°C respectively.

Grain sizes (G') were measured using an image analyser "Seescan" which measures the Feret diameter[1] of each grain. The hardness data obtained from the heat treated samples are listed in Tables 5.4 and 5.5 respectively.

From the hardness results listed in Table 5.5, it can be seen that annealing the specimens at 1100°C for up to 230400 seconds does not show any significant decrease in hardness, when compared with the hardness changes obtained after annealing at relatively high temperatures and for shorter time periods. These hardness results are better illustrated graphically in figure 5.15. This is consistent with the earlier conclusions that no recrystallisation occurs at peak temperatures below 1160°C during zone annealing and is probably again related to the lack of γ' dissolution. Optical microscopy (figure 5.16) revealed no significant change in microstructure after annealing at 1100°C.

On the other hand, after annealing at 1200 and 1300°C, it is evident from figures 5.17 & 5.18, that these samples show a fully recrystallised grain structure even after very short annealing periods.

Table 5.4, which shows the average grain size (G') as measured on the longitudinal sections of specimens annealed at 1200 and 1300°C. Although the measurement errors are fairly large (Table 5.4), a relatively smaller grain size is recorded after isothermal annealing at 1300°C when compared

[1] Feret diameter can be explained as average of diameter of each grain along 36 different directions and 10° with respect to each other.

with that recorded after isothermal annealing at 1200°C. This is consistent with the hardness data enumerated in Table 5.4, which shows that after annealing at 1300°C for 900 seconds, the hardness recorded is slightly higher than when annealed at 1200°C for same period of time. The reason for this behaviour are not understood, but the main conclusion from these experiments is the MA6000 does not directionally recrystallise during isothermal annealing, so that the influence of oxide particle alignment induced during working is rather small.

Table 5.4. Illustrating average grain size (mm), after isothermal annealing MA6000 at different temperatures and time. The quantities given in brackets indicate the standard deviation of the measurements.

Temperature	Annealing time in seconds						
°C	900	1800	3600	7200	14400	28800	57600
	Average grain size (mm) G'						
1200	0.15	0.15	0.15	0.23	0.18	0.20	0.18
	(0.02)	(0.02)	(0.02)	(0.03)	(0.03)	(0.03)	(0.02)
1300	0.13	0.11	0.14	0.15	0.13		
	(0.02)	(0.01)	(0.02)	(0.02)	(0.01)		

Table 5.5. Hardness (HVN) data obtained after isothermal annealing MA6000 at different temperatures and time.

Temperature	Annealing time in seconds								
°C	900	1800	3600	7200	14400	28800	57600	115200	230400
	Hardness HV								
1100	634	606	613	606	613	613	613	585	519
	649	613	620	627	620	613	613	579	525
	657	634	634	613	620	613	613	599	525
	642	627	620	634	613	613	606	599	525
	634	613	606	613	613	613	606	592	519
	Mean hardness values								
	643	619	619	619	616	613	610	591	523
1200	503	488	498	498	503	493	473		
	519	525	514	514	508	503	498		
	525	519	508	514	508	498	514		
	508	519	483	483	488	508	514		
	503	488	503	498	503	503	503		
	Mean hardness values								
	512	508	501	501	502	501	500		
1300	508	468	498	519	478				
	514	530	525	525	508				
	519	548	530	514	498				
	542	530	508	498	519				
	519	508	498	478	519				
	Mean hardness values								
	520	517	512	507	504				

5.10 Conclusions

It appears that there is a well-defined recrystallisation temperature (around 1160°C) for MA6000, below which no recrystallisation was observed during zone annealing or isothermal annealing experiments, at least for the range of conditions considered. This may be related to the fact that γ' only dissolves beyond that temperature. Some evidence for this was revealed by the modified morphology of γ' observed in the recrystallised samples.

It is found possible to directionally recrystallise the Inconel alloy MA6000 in both parallel and perpendicular directions to the rolling direction. However, the degree of grain isotropy is much higher in the latter case, because of the presence of the aligned rows of particles along the working direction, which enhance growth along that direction.

From the range of zone annealing experiments performed at variety of peak temperatures and specimen travel speeds, it is found possible to control the grain size by recrystallising at a suitable temperature and speed.

Isothermal annealing experiments have confirmed that the lack of recrystallisation in superalloy MA6000, below 1100°C, and this is probably a reflection of the lack of γ' dissolution below that temperature. Furthermore, directional recrystallisation was not observed in any sample after isothermally annealing, the recrystallised microstructures always appearing equiaxed. It is concluded, therefore, that the influence of any particle alignment in the alloy is rather minor.

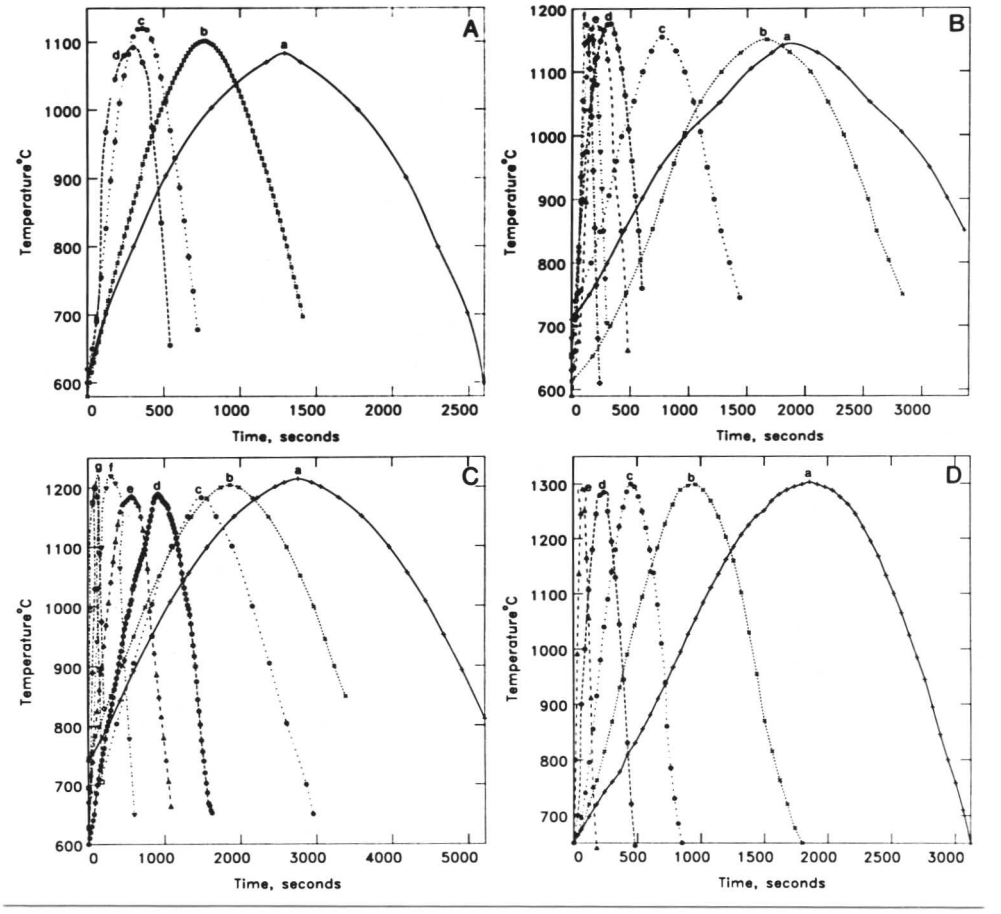

Figure 5.3. Measured time versus temperature curves for the data recorded during zone annealing of Inconel alloy MA6000.

a. T_p = 1100°C, profiles a-d represent specimen travel speeds 0.8, 1.4, 3.2 and 5.0 mm/min respectively.

b. T_p = 1160°C, profiles a-f represent specimen travel speeds 0.8, 1.4, 3.2, 5.0, 7.7 and 10.0 mm/min respectively.

c. T_p = 1200°C, profiles a-g represent specimen travel speeds 0.4, 0.8, 1.4, 3.2, 5.0, 7.7 and 10.0 mm/min respectively.

d. T_p = 1300°C, profiles a-f represent specimen travel speeds 0.8, 1.4, 3.2, 5.0, 7.7 and 10.0 mm/min respectively.

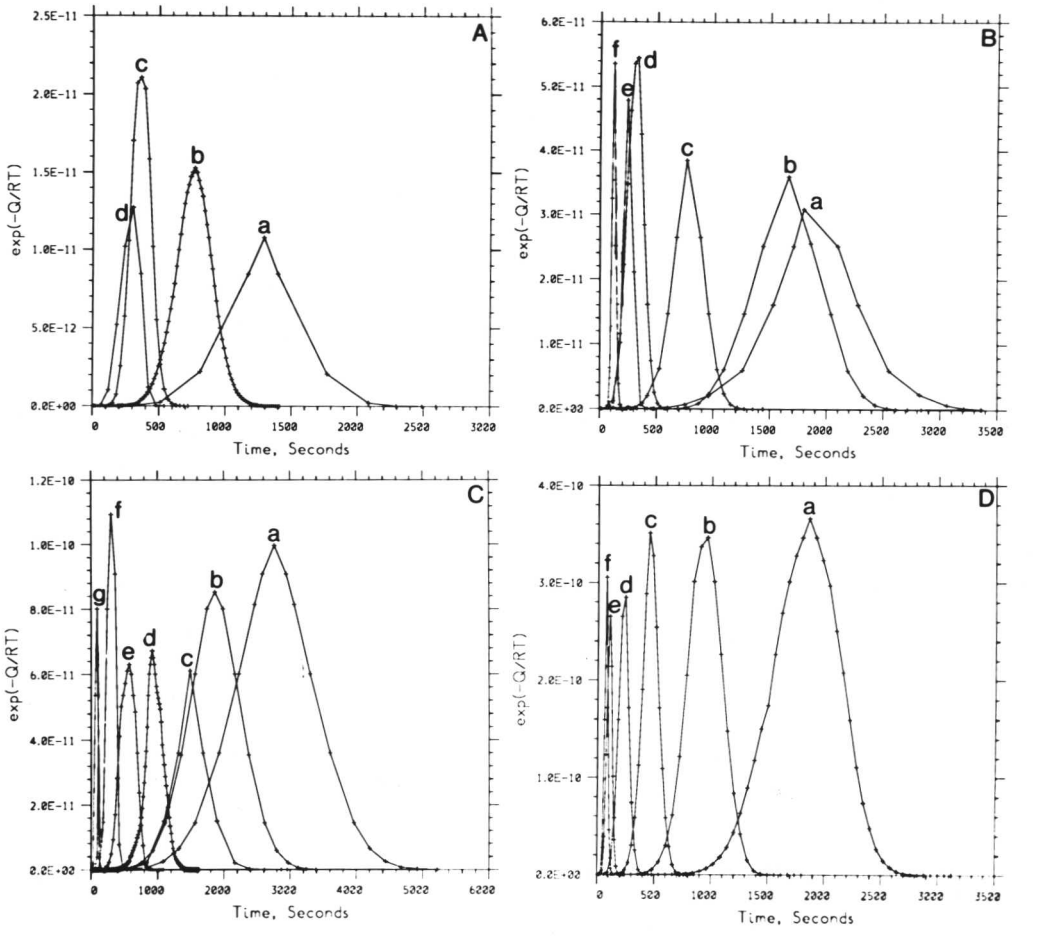

Figure 5.4. Calculated values of the term exp(-Q/RT) versus time as recorded during zone annealing experiments.

a. T_p = 1100°C, profiles a-d represent specimen travel speeds 0.8, 1.4, 3.2 and 5.0 mm/min respectively.

b. T_p = 1160°C, profiles a-f represent specimen travel speeds 0.8, 1.4, 3.2, 5.0, 7.7 and 10.0 mm/min respectively.

c. T_p = 1200°C, profiles a-g represent specimen travel speeds 0.4, 0.8, 1.4, 3.2, 5.0, 7.7 and 10.0 mm/min respectively.

d. T_p = 1300°C, profiles a-f represent specimen travel speeds 0.8, 1.4, 3.2, 5.0, 7.7 and 10.0 mm/min respectively.

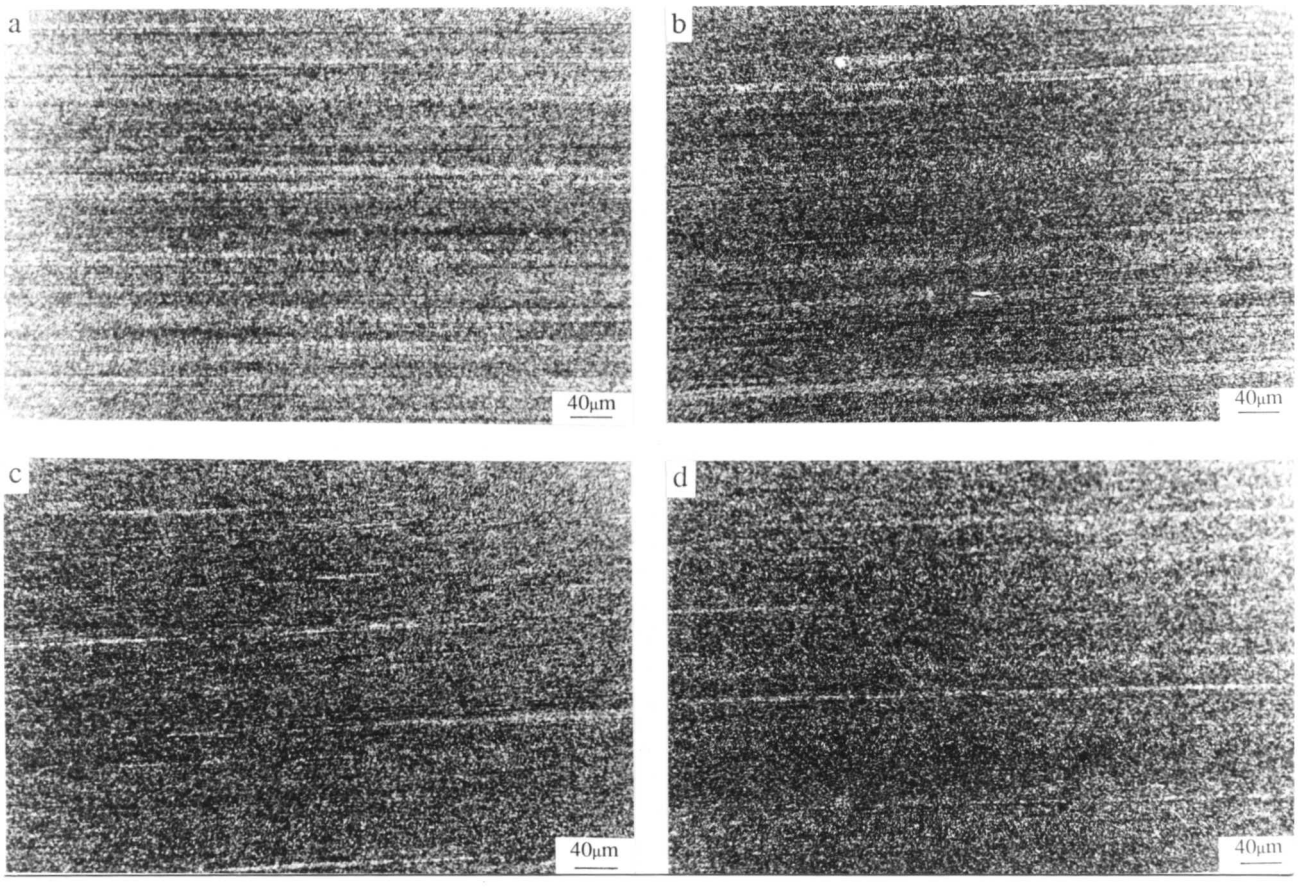

Figure 5.5. Micrographs taken after zone annealing MA6000 at T_p = 1100°C. The specimen travel speeds and hardness data are as follows:

a. 0.8 mm/min, mean HV 615

b. 1.4 mm/min, mean HV 624

c. 3.2 mm/min, mean HV 637

d. 5.0 mm/min, mean HV 639

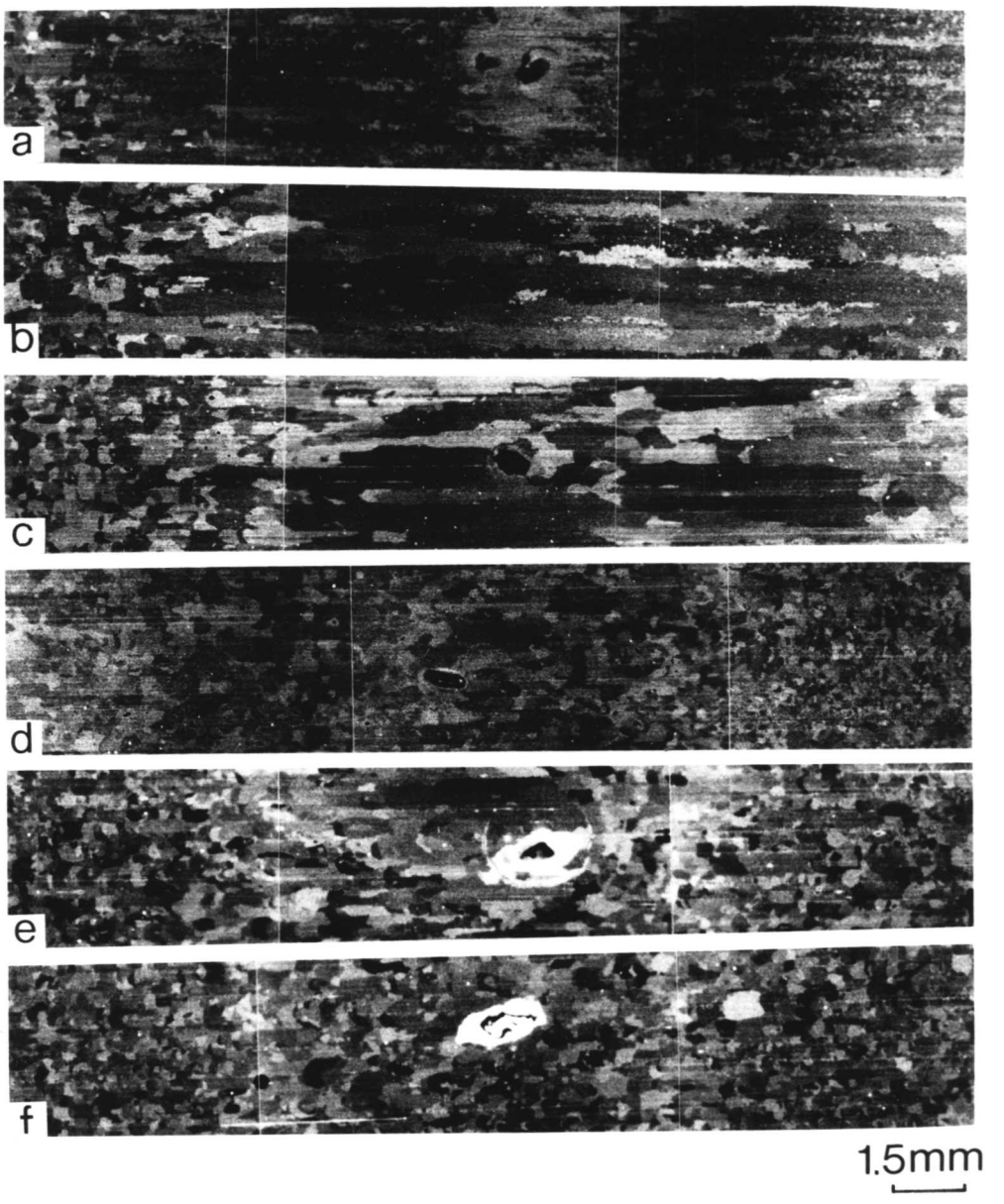

Figure 5.6. Microstructure recorded after zone annealing MA6000 at T_p = 1160°C, with different specimen travel speed.

a. 0.8 mm/min, mean HV 496 b. 1.4 mm/min, mean HV 499

c. 3.2 mm/min, mean HV 517 d. 5.0 mm/min, mean HV 520

e. 7.7 mm/min, mean HV 527 f. 10.0 mm/min, mean HV 534

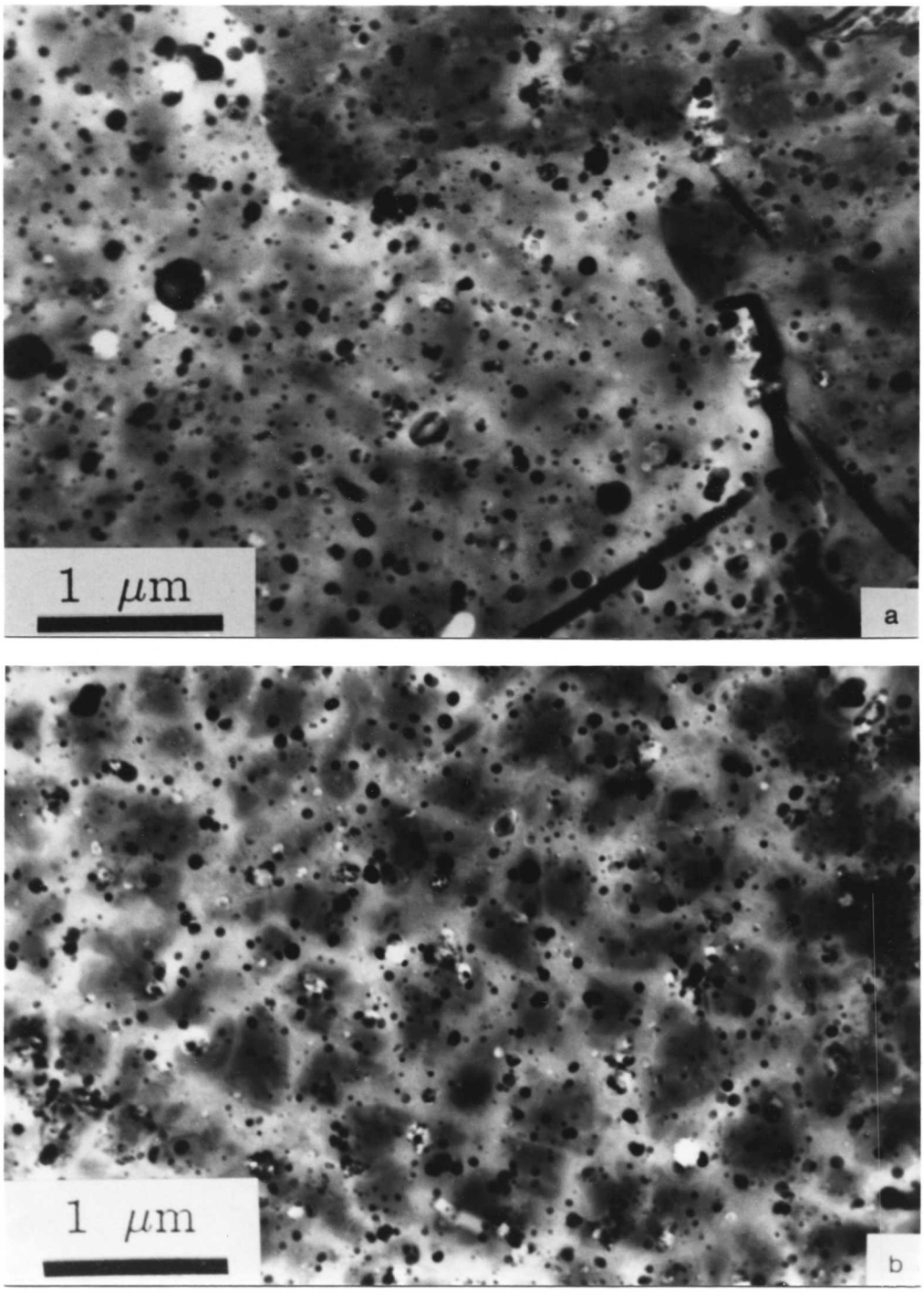

Figure 5.7. Electron micrographs recorded on the examination of thin foil prepared from the longitudinal section of the specimen zone annealed at T_p = 1160°C, with specimen travel speed of 5 mm/min.

a. Bright field image illustrating grain boundary in directionally recrystallised sample of MA6000, no alignment of particles can be seen on or along the grain boundary.

b. Bright field image showing random distribution of particles in the matrix.

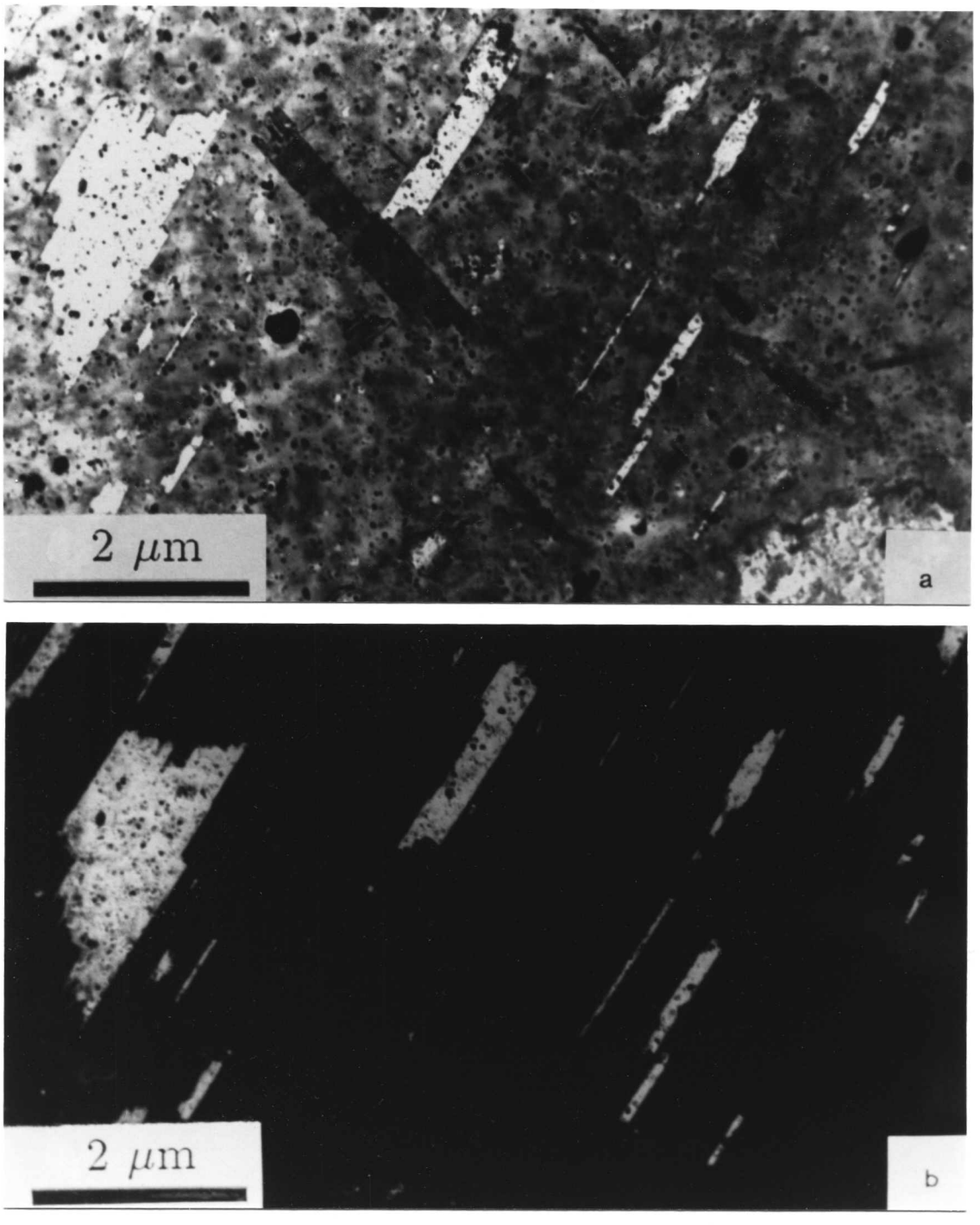

Figure 5.8. Transmission electron micrographs recorded on the examination of thin foil prepared from the longitudinal section of the specimen zone annealed at T_p = 1160°C, with specimen travel speed of 5 mm/min.

a. Bright field image showing annealing twins in a directionally recrystallised grain of nickel base superalloy MA6000.

b. Corresponding annealing twins dark field image.

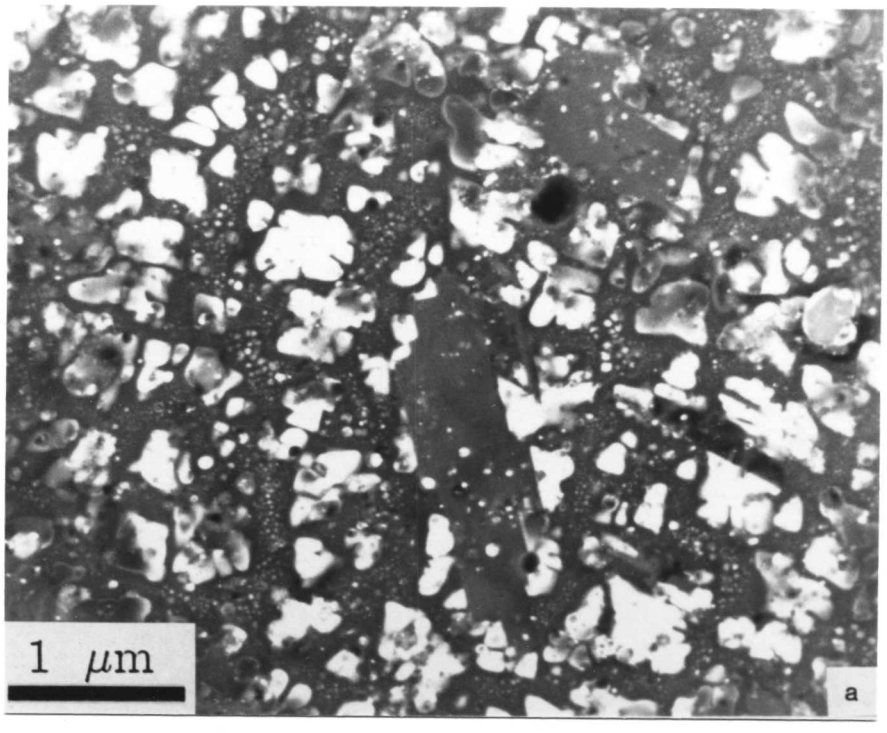

Figure 5.9. Transmission electron micrograph showing dendritic shaped γ' precipitate in nickel base superalloy MA6000, after zone annealing at T_p = 1160°C, with a specimen travel speed of 5 mm/min.

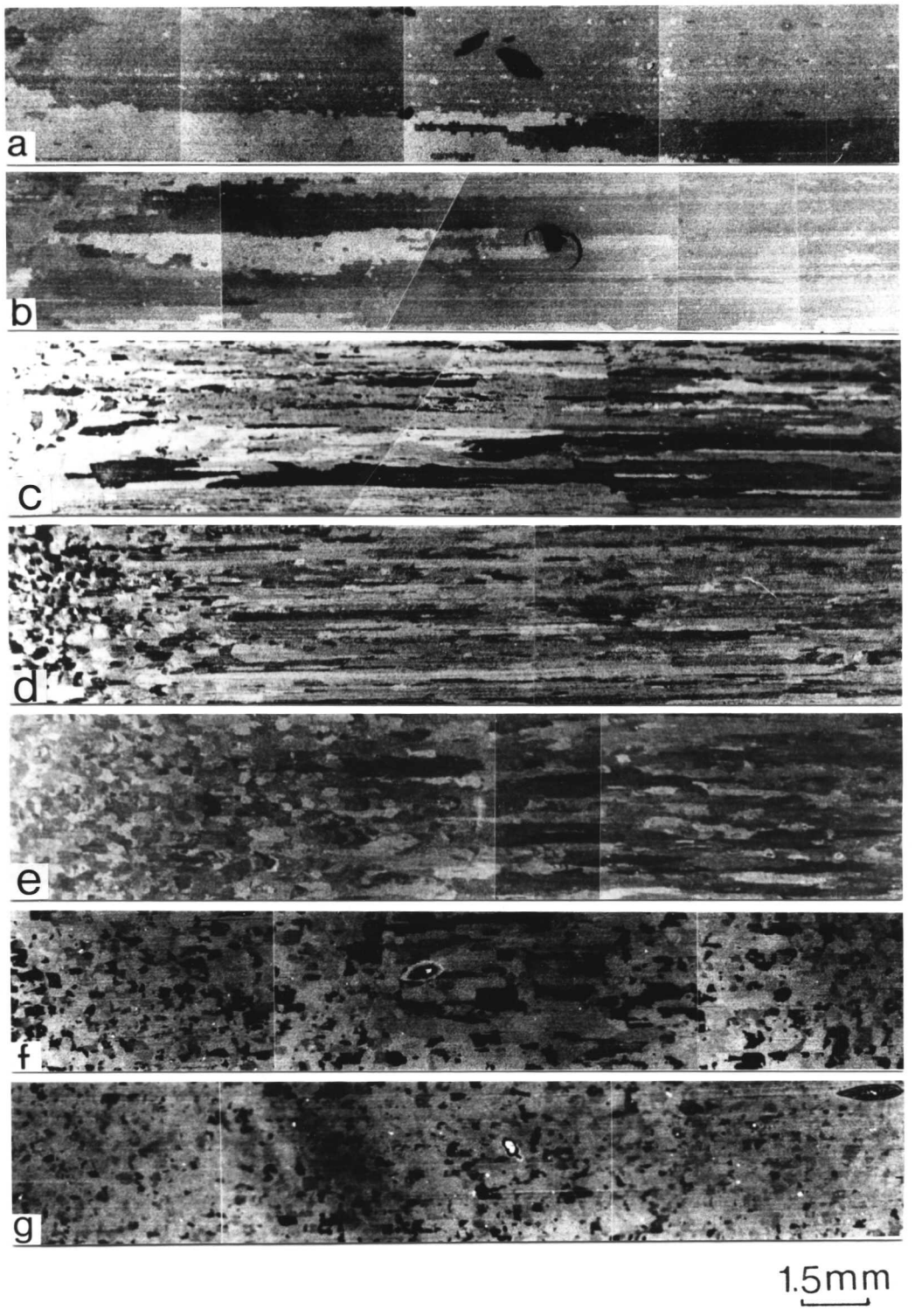

Figure 5.10. Showing the microstructure of MA6000, after zone annealing at T_p = 1200°C. The specimen travel speeds and hardness data are as follows:

a. 0.4 mm/min, mean HV 476 b. 0.8 mm/min, mean HV 488 c. 1.4 mm/min, mean HV 482

d. 3.2 mm/min, mean HV 490 e. 5.0 mm/min, mean HV 486 f. 7.7 mm/min, mean HV 524

g. 10.0 mm/min, mean HV 528

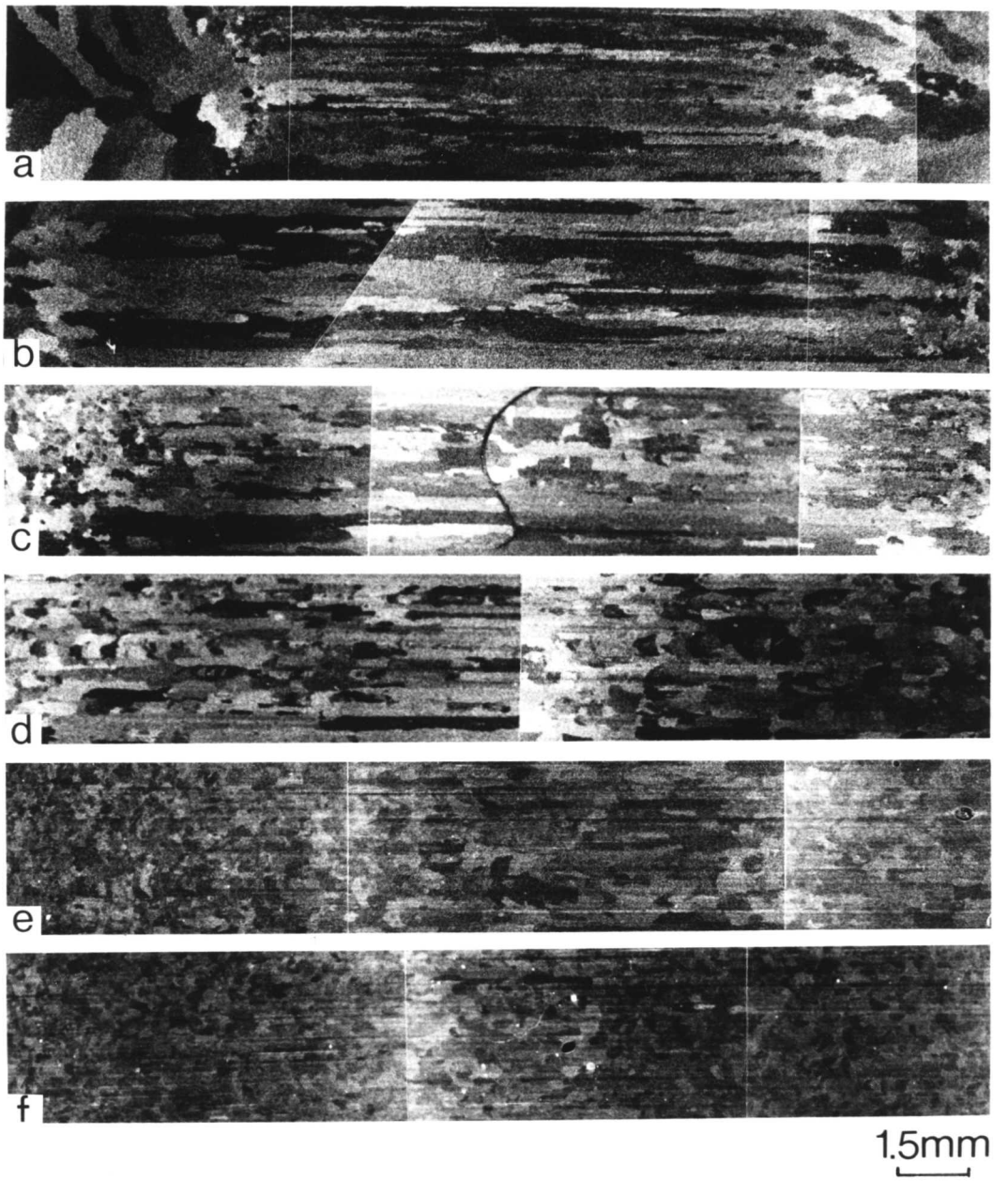

Figure 5.11. Showing the microstructure obtained after zone annealing samples at T_p = 1300°C. The specimen travel speeds and hardness data are as follows:

a. 0.8 mm/min, mean HV 420
b. 1.4 mm/min, mean HV 489
c. 3.2 mm/min, mean HV 469
d. 5.0 mm/min, mean HV 489
e. 7.7 mm/min, mean HV 499
f. 10.0 mm/min, mean HV 512

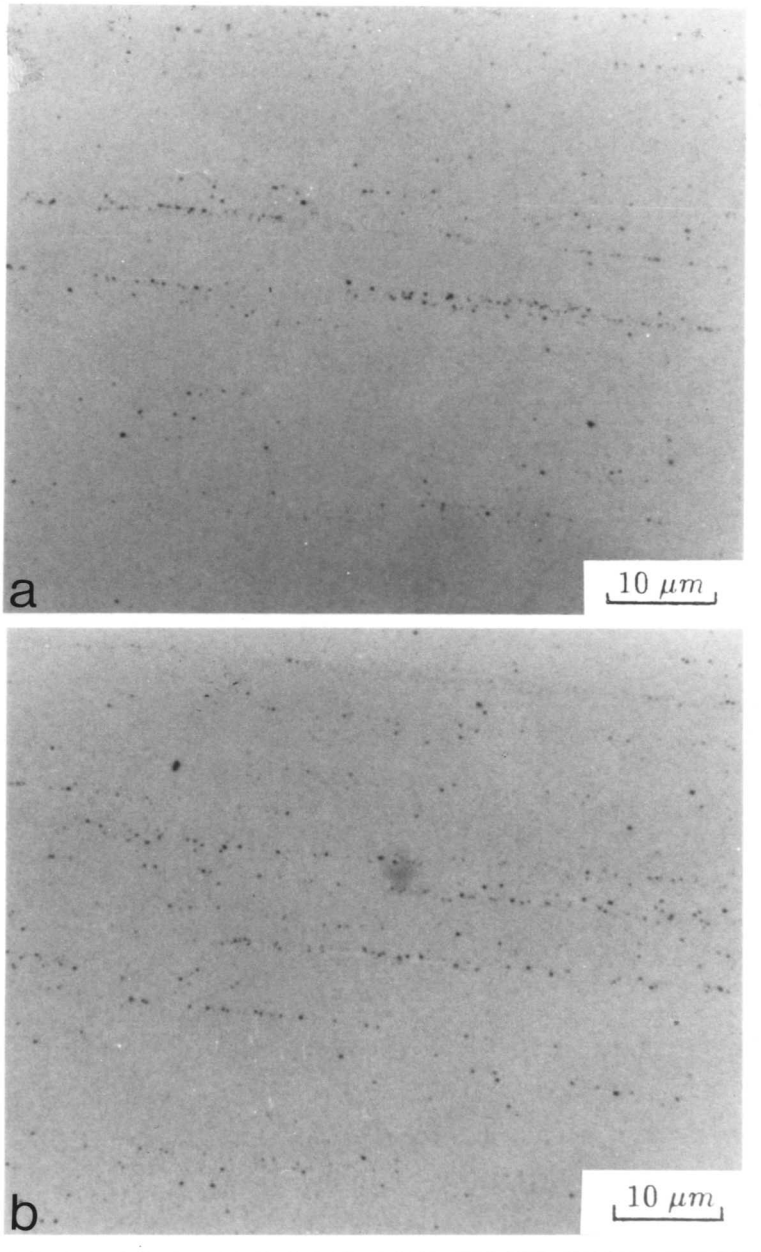

Figure 5.12. Shows some alignment of particles of yttrium oxide in samples of alloy MA6000, in as-received condition. The sample is unetched.

a. Grinding and polishing, parallel to the rolling direction

b. Grinding and polishing, perpendicular to the rolling direction.

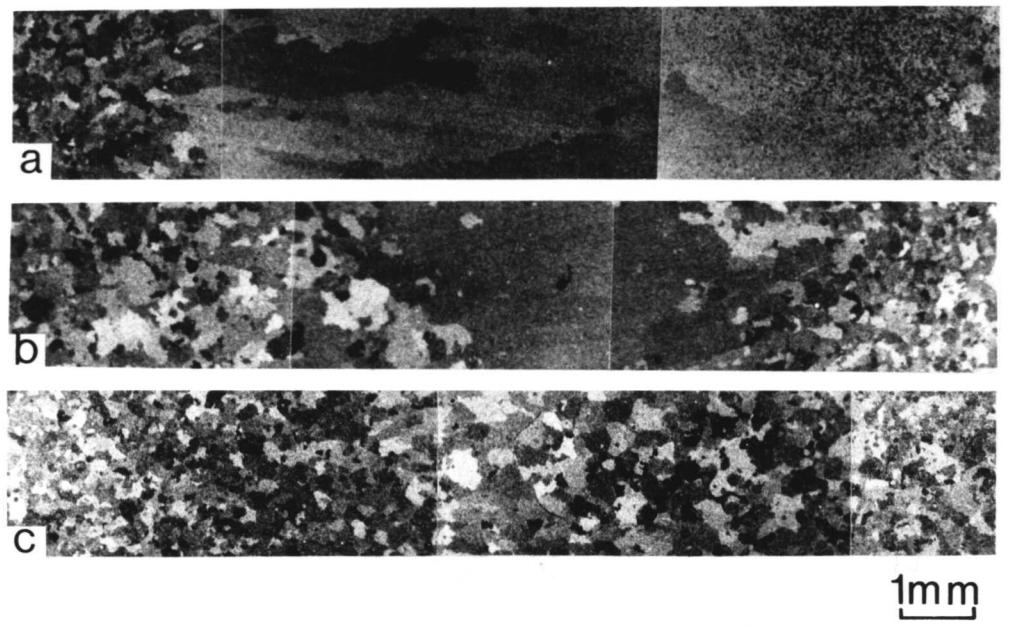

Figure 5.13. Showing the microstructure recorded after zone annealing. The specimens were prepared with the zone annealing direction perpendicular to the rolling direction at T_p = 1200°C.

a. 1.4 mm/min, HV 508 b. 3.2 mm/min, HV 523 c. 5.0 mm/min, HV 533

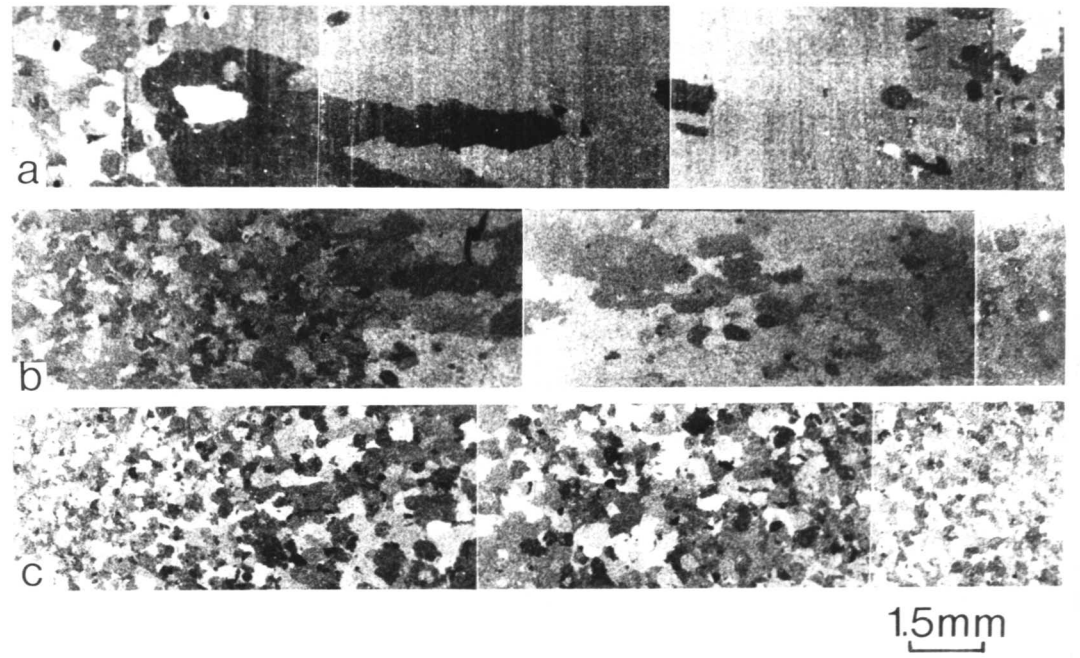

Figure 5.14. The microstructure recorded after zone annealing (at T_p = 1300 °C) specimens in a direction perpendicular to the rolling direction.

a. 1.4 mm/min, HV 482 b. 3.2 mm/min, HV 503 c. 5.0 mm/min, HV 513

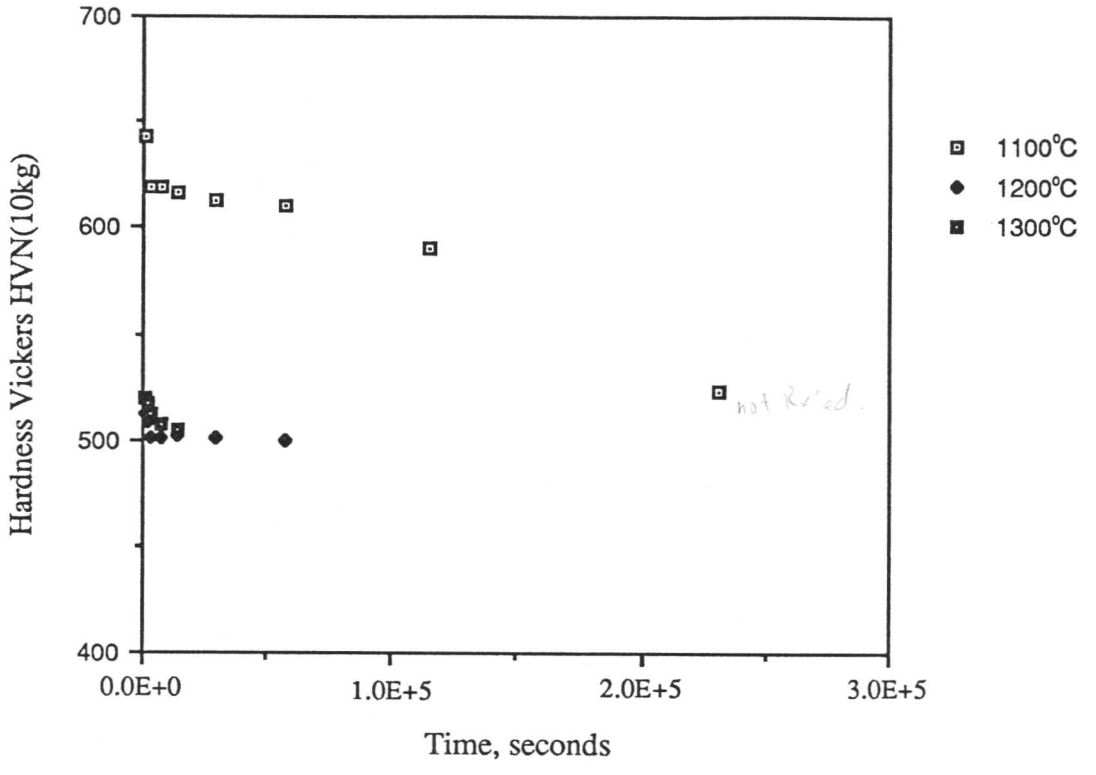

Figure 5.15. Graphic representation of hardness results obtained after isothermal annealing MA6000 at temperatures ranging from 1100 to 1300°C for different periods of time. Note that the hardness of the samples annealed at 1300°C in general trends to be higher than that of the samples annealed at 1200°C.

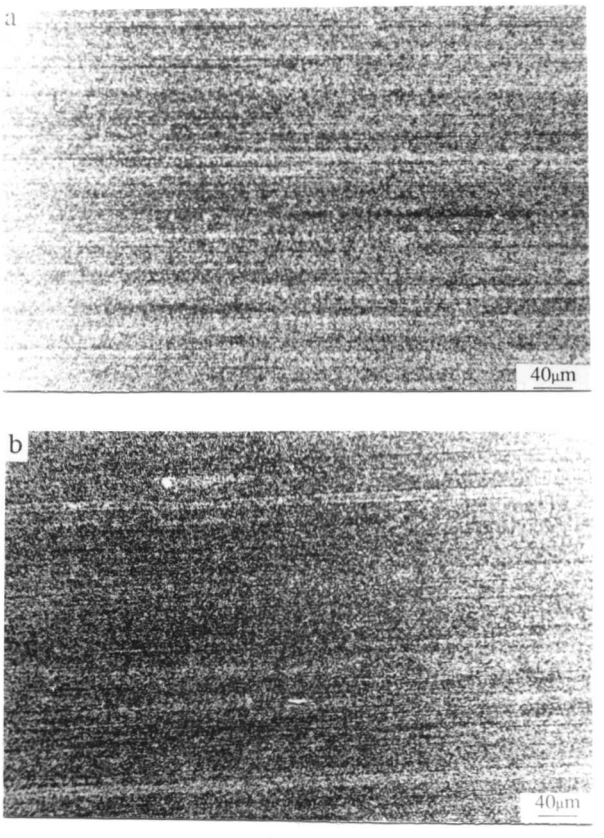

Figure 5.16. Optical micrographs taken after isothermally annealing specimens from alloy MA6000 at 1100°C for:

a. 900 seconds, HV 634

b. 230400 seconds, HV 522

The indentation load applied was 10kg.

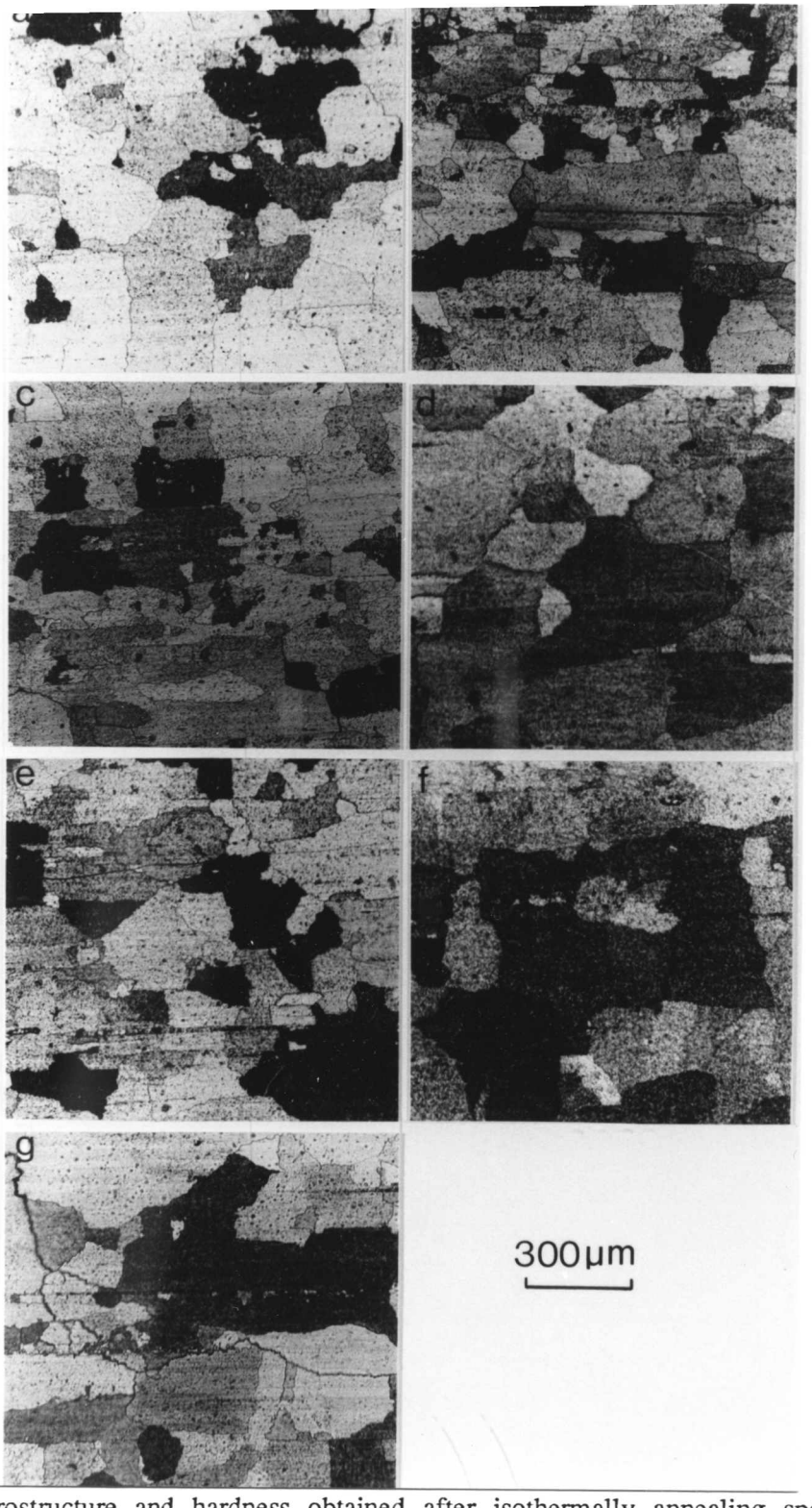

Figure 5.17. Microstructure and hardness obtained after isothermally annealing specimens from MA6000 at 1200°C for:

a. 900 s, HV 511
b. 1800 s, HV 507
c. 3600 s, HV 501
d. 7200 s, HV 501
e. 14400 s, HV 502
f. 28800 s, HV 501
g. 57600 s, HV 500

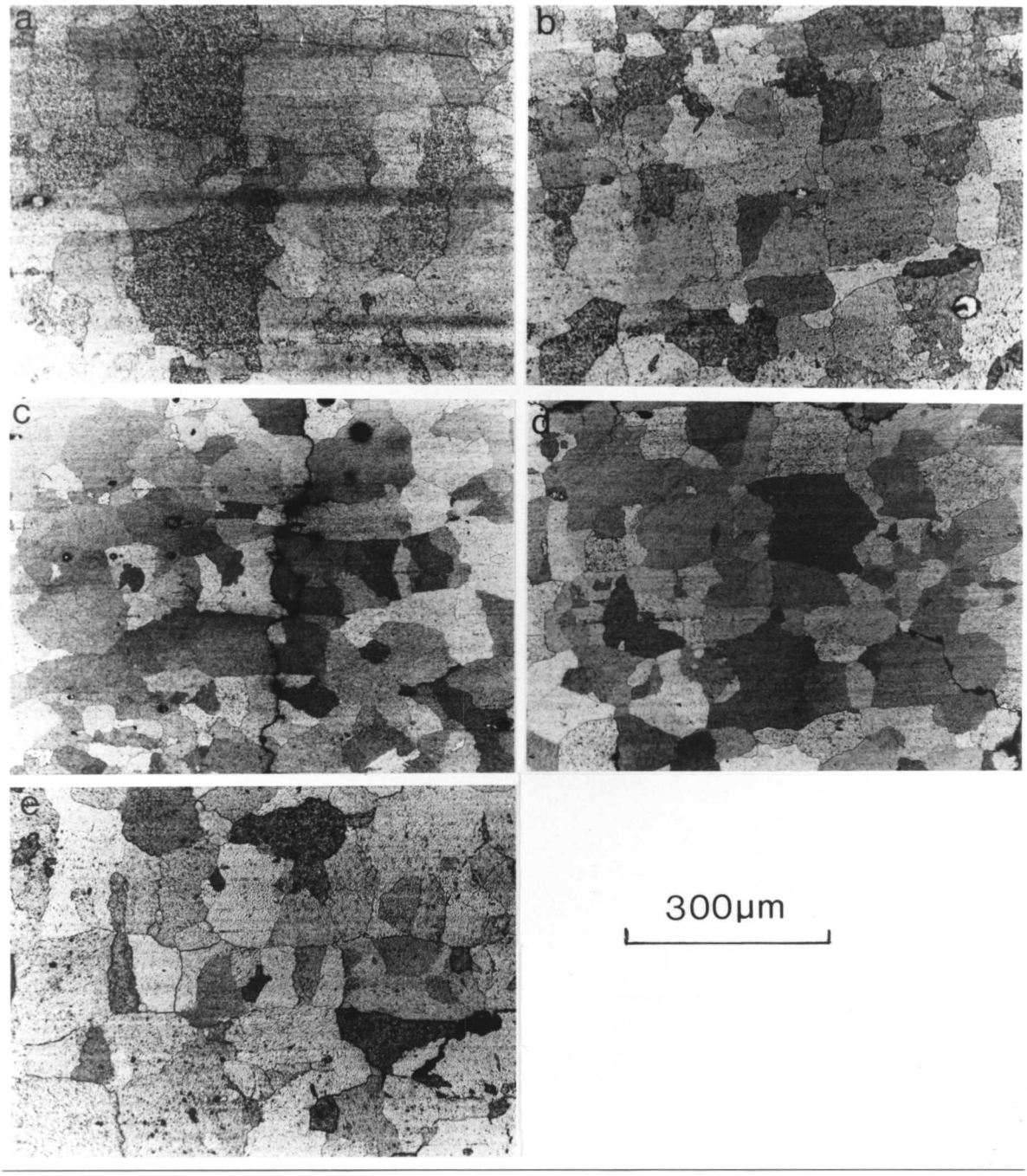

Figure 5.18. Optical micrographs recorded after isothermally annealing specimens from MA6000 at 1300°C for:

a. 900 s, HV 520
b. 1800 s, HV 516
c. 3600 s, HV 511
d. 7200 s, HV 506
e. 14400 s, HV 504

CHAPTER SIX

Zone Annealing and Isothermal Annealing Experiments Performed on Oxide Dispersion Strengthened Ferritic Steel Incoloy MA956

6.1 Introduction

For medium temperature applications, such as gas turbine components, a ferritic composition offers certain distinct advantages over nickel base superalloys which are superior at high temperatures. The melting point of Fe-Cr alloys, for example, is generally over 1480°C, well above that of typical Ni-base alloys. The density of a body-centred-cubic iron base alloy is at least 10% lower than a face-centred-cubic alloy providing a significant strength to weight advantage. Furthermore, ferritic compositions are characterised by lower thermal expansion coefficient than Ni-base alloys which should be beneficial to thermal fatigue life (Fischer et al., 1977).

For more than a decade, oxide dispersion strengthened superalloys have been under intensive development to exploit their potential for better creep resistance and stability at very high temperatures (Hack, 1984). While a significant effort has been expended on oxide dispersion strengthened nickel base superalloys, relatively little work has been done on iron-base, ferritic materials for high temperature use.

The most highly developed steel, Incoloy alloy MA956 is an oxide dispersion strengthened Fe-Cr-Al alloy produced by the mechanical alloying technique, which is explained in detail by Benjamin (1970). The alloy is strengthened by an yttrium oxide dispersoid that remains stable at temperatures up to the melting point of the material. The oxide particle size is reported for Incoloy MA956 to range from 20 to 40nm (Hack, 1988). It has also been suggested by Huet et al. (1979), that the oxide dispersion tends to stabilise the subgrain boundaries which contribute also for a significant part to the strength of the alloy.

The chemical composition of alloy MA956, used to study directional recrystallisation in the present work, is listed in Table 6.1 (also see Table 3.1).

The material is prepared by mechanical alloying using elemental iron powder and Fe-Cr-Al-Ti master alloy crushed to 150 μm; the Y_2O_3 powder is added and at this stage the whole mixture is

hot compacted by extrusion.

Table 6.1. Chemical composition of Inconel Alloy MA956.

Alloy designation	Chemical composition (wt%)				
	Cr	Al	C	Y_2O_3	Balance
MA956	19.88	4.52	0.014	0.52	Fe

The properties, microstructure and other characteristics of ODS Fe-Cr-Al alloys, and their recrystallisation behaviour are first reviewed and attention is then turned to the experimental results obtained after performing zone annealing and isothermal annealing experiments, the aim of which was to achieve and understand the directional recrystallisation behaviour of the alloy.

6.2 Properties of MA956

MA956 in the form of bar and sheet exhibits a high stress-rupture strength (e. g., 67 MN m^{-2} at 982°C for 1000 hours life, in the form of sheet (Incomap)). As a consequence of its exceptionally high aluminium content, the high strength capability is combined with exceptional high temperature oxidation and corrosion resistance, associated with the formation of an aluminium oxide scale. MA956 also has a good cyclic oxidation resistance. The alumina scale is an excellent barrier to carbon in situations where carburisation occurs in hydrogen-methane mixtures at 1000°C, and this makes an alloy useful in systems designed to convert gas into electricity. Sulphidation resistance is also known to be good (Fleetwood, 1986). Figure 6.1 shows the stress-rupture properties of MA956 at 982°C and 1093°C, as reported by Fischer et al. (1977).

The strength properties of this alloy (MA956) are rather similar to the ODS Ni-alloys discussed earlier and it possesses superior high gas velocity oxidation resistance at 1165 K (892°C) when compared with the Ni-base alloys (Whittenberger, 1979).

6.3 Microstructure of ODS Fe-Cr-Al Alloys

Secondary recrystallisation (Aust, 1963), or exaggerated grain growth in oxide dispersion strengthened materials leads to anisotropic grain size with high aspect ratio (l/d). In most cases the ratio of longitudinal diameter (l) to transverse diameter (d) should generally be greater than 3 to produce substantial improvements in high temperature properties. Under ideal conditions the aspect ratio may exceed ten (Schilling, 1977).

The grain structure of dispersion strengthened Ni-base alloys produced by mechanical alloying is generally characterised by coarse, elongated grains (Benjamin, 1970 and Cairns, 1974). This type of grain structure is developed during high temperature annealing treatment by a process resembling secondary recrystallisation. It has been shown that the presence of coarse elongated grain structure is vital to attain the good high temperature stress rupture properties (Wilcox and Clauer, 1972) by providing fewer density of easy diffusion path along the major stress axis parallel to the long directions of the grains.

Fischer et al. (1977), have attempted to study the structure and properties of a newly developed dispersion strengthened ferritic alloy, designated MA956E, in sheet form, having chemical composition Fe-19.1Cr-4.6Al-0.50Ti-0.50Y_2O_3-0.26O-0.042N wt%. They observed large, pancake shaped grains which were approximately equiaxed in the plane of the sheet, with grain diameters exceeding 5mm. They also examined the surface parallel to the rolling direction of the annealed sheet, and found a highly elongated grain structure. The thickness of the grains was found to be in the range 0.2 - 0.5mm, with an aspect ratio of > 10 for both the longitudinal and transverse directions in the plane of the sheet. They also found some very fine elongated grains within the large pancake shaped grains and assumed that these regions corresponded to remnant areas of misorientation that recrystallise independently, and which cannot be accommodated by the sweeping boundary that produces the large grains.

Ubhi et al. (1981), also studied the microstructure of MA956E in the form of hot-extruded bar (the chemical composition was slightly different at Fe-18.55Cr-4.5Al-0.33Ti-0.032C-0.42Y_2O_3wt%.) Using light microscopy they found a relatively fine elongated grain structure in the as-deformed sample, with a wide variation in grain size. At higher magnification using transmission electron microscopy, they observed very variable but usually elongated grains in both the longitudinal and extrusion plane sections. Despite large variations in shape, they observed that most of the grains were cigar-shaped with a length of about 1μm and a diameter of 0.5μm. They also observed a variable density and distribution of dislocations from grain to grain. From all these observations, they concluded that during the hot extrusion stage, dynamic recovery and recrystallisation occur to produce a mixture of elongated deformed grains and relatively equiaxed recrystallised grains. They identified the second phase particles present in the bar using X-ray and electron diffraction as,

a) yttrium aluminate ($3Y_2O_3.5Al_2O_3$) - uniformly distributed fine spherical particles with an average size of 30nm;

b) titanium nitride (TiN) - angular particles with an average size of 200nm situated mainly, but not exclusively, on the grain boundaries;

c) alumina (α-Al_2O_3) - occasionally arranged as long stringers, but otherwise as coarse irregular particles ranging in size from 0.5 to 1 μm.

According to Wilson et al. (1978), the most significant change which occurs during sintering and extrusion is the formation of yttrium aluminate by reaction of fragmented yttria particles with the aluminium available in solid-solution, and oxygen in air, in the can or from the decomposition of fragmented oxides of master alloy. Surplus oxygen is certainly available within the system since free α-aluminium oxide is also formed at this stage (Whittenberger, 1978).

6.4 Material

The material for the present work was supplied in the hot-rolled condition with no heat treatment applied subsequent to fabrication, in the form of bar with 25mm diameter and 1000mm length. The hot-rolling was done at 1000°C in one heat from 54 mm diameter to 25 mm diameter (an 54% reduction). Specimens for further work were cut in the form of square rods of dimension 5 x 5 x 20mm with the length direction parallel to the rolling direction, and others were prepared with the long dimension perpendicular to the rolling direction. The details of equipment used for zone annealing are given in chapter 3.

The zone annealing experiments have been performed at five different peak temperatures ranging from 1180 to 1380°C, using eight constant specimen travel speeds for each peak temperature (0.2, 0.4, 0.8, 1.4, 3.2, 5.0, 7.7, 10.0 mm/min).

The initial microstructure (as-deformed) has been discussed in detail for MA956 in chapter 4.

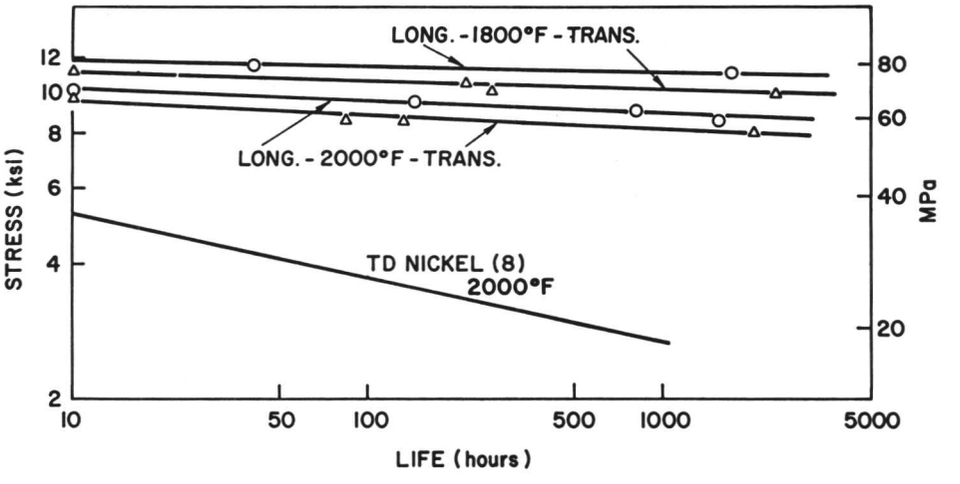

Figure 6.1. Stress-rupture curves from experiments conducted at 980°C and 1090°C for MA956E sheet, after Fischer et al. (1977).

6.5 Results

The results obtained in the form of microstructure and hardness tests, after zone annealing MA956 are listed in Table 6.2.

From the optical micrographs shown in figure 6.7, which were recorded after zone annealing the specimens at T_p = 1150°C, with specimen travel speeds 0.2, 0.4, 1.4, 3.2, 5.0, 7.7 and 10.0 mm/min, only a very small amount of directional recrystallisation could be seen at even the slowest travel speed (0.2 mm/min) utilised. This indicates that at relatively lower peak temperatures (1150°C or less) longer time periods (not accessible with our equipment) are required to fully directionally recrystallise the samples of alloy MA956.

From figures 6.8a, b, c & d, which were recorded after zone annealing samples at T_p = 1180°C with specimen travel speeds 0.8, 1.4, 3.2 and 5.0 mm/min respectively, it can be seen that the faster specimen travel speeds have no significant effect on the microstructure, but as the speed drops to 1.4 mm/min, the alloy partially recrystallises and until at the slower speed of 0.8 mm/min a fully grown columnar grain structure is produced (figure 6.8a). It was observed (figure 6.8c & d), that the samples did not exhibit any equiaxed grain structure at the specimen ends when prepared and zone annealed parallel to the rolling direction. Under the same conditions, those samples which were zone annealed, after being prepared normal to the rolling direction, exhibited an equiaxed grain shape at a specimen travel speed of 1.4 mm/min. Further increases in specimen travel speeds produced only partially recrystallised grain structures (see Table 6.2a & figure 6.16).

These differences in behaviour could be a consequence of the fabrication process. An attempt was made to show the effect of particle alignment on the recrystallisation of MA956, alignment which can be seen in figure 6.9, which was taken from an unetched specimen zone annealed at T_p = 1280°C and 1.4 mm/min. It is apparent that some of the particles are aligned along the deformation direction, the spacing between adjacent rows of aligned particles being approximately equal to the maximum lateral spacing observed between two adjacent grain boundaries in directionally recrystallised specimens.

The transmission electron micrograph shown in figure 6.10, recorded from the longitudinal section (parallel to the rolling direction) of the sample zone annealed at T_p = 1180°C (0.8 mm/min), further confirms the effect of particles on the directional recrystallisation process for MA956, which directionally recrystallises even during isothermal annealing. From figure 6.10, it can be seen that the very fine and relatively coarser particles are aligned along the grain boundary,

which was found after considerable effort because of large grain size (Table 6.3) obtained after zone annealing. Figure 6.11 illustrates the microstructure observed using transmission electron microscopy on a sample zone annealed at T_p = 1280°C (3.2 mm/min). It can be seen that the small particles have a pinning effect on the grain boundary but not to an extent which prevents recrystallisation. Occasionally, streams of unrecrystallised regions were found between nearly fully recrystallised, dislocation "free" grains. This happened at the faster specimen travel speed (3.2 mm/min), where recrystallisation front moves relatively rapidly so that any regions which are pinned will be left behind and may leave the hot zone before unpinning can occur. Such effect could not be revealed using optical microscopy which indicates full recrystallisation (figure 6.12c).

The microstructural results obtained after zone annealing at T_p = 1180°C, from the specimens prepared parallel to the rolling direction were found to be in good agreement with the hardness results. It can be seen from Table 6.2a, and figures 6.8a - d that as the specimen travel speed decreases and the material undergoes recrystallisation, the hardness values correspondingly decrease.

The data for T_p = 1180°C reported in Table 6.2a, in effect give an experimental measurement of the grain boundary movement rate since there is a transition from a fully directionally recrystallised microstructure to one which contains some recrystallised grains in a partially recrystallised sample. At the speeds higher than the transition speed, the recrystallisation front cannot keep up with the motion of the sample and only partial recrystallisation is achieved, the boundaries could, within the confines of the hot zone, move at rates higher than the specimen travel speed. The partially recrystallised samples show that there is no difficulty in nucleating new grains, but because these grains are unable to keep up with the motion of the sample, only partial recrystallisation obtains. Thus, for the partially recrystallised sample, the specimen speed gives an upper limit to the grain boundary velocity in the direction of specimen travel.

Assuming that columnar growth can only be sustained if the interface velocity I_v is equal to or greater than the specimen travel speed T_v,

we have,

$$I_v < T_v \rightarrow \text{partial recrystallisation}$$

and if,

$$I_v << T_v \rightarrow \text{deformed state remains}$$

and if,

$$I_v \geq T_v \quad \rightarrow \quad \text{directional recrystallisation follows}$$

Now grain boundary rate theory for isothermal conditions gives (Christian, 1975),

$$I_v = \delta^B \nu(-\Delta_a g^* / kT) [1-\exp(-\Delta g^{\beta\alpha})] \qquad .....(6.1)$$

I_v	interface velocity
δ^B	thickness of boundary ~ size of 1 atom
ν	atomic vibration frequency
$\Delta_a g^*$	free energy of activation, (especially for incoherent growth)
$\Delta g^{\beta\alpha}$	driving force per atom (from β to α), where β and α refer to the recrystallised and deformed grains respectively
k	Boltzmann constant J/K
T	absolute temperature

now,

$$\nu = kT / h \qquad .....(6.2)$$

Where h is the Planck constant.

Since the driving force for recrystallisation is constant and independent of temperature, and since the other terms apart from temperature are also in effect constant, the above equation (6.1) reduces to the form

$$I_v \propto \exp \{ -Q / RT \} \qquad .....(6.3)$$

where Q is an activation energy.

An attempt has been made to deduce the activation energy Q from the experimental data on directionally recrystallised samples. The equations discussed above deal with the motion of a grain boundary under isothermal conditions, whereas, zone annealing clearly involves a complicated continuous heating and cooling cycle.

One way of taking this into account could be by using the concept of the "kinetic strength" of an anisothermal heat treatment. This concept has been used for many decades in the form of the Hollomon-Jaffe tempering parameter (Hollomon and Jaffe, 1945) and has in recent years been re-emphasised in the modelling of the heat-affected zones of steel weld deposits by Ashby and Easterling (1982). In essence, the kinetic strength of a heat treatment is indicated by integrating the exponential function over the range of the heat treatment. The concept may be applied in the present work by deducing the minimum value of kinetic strength, $D = D_E$, required to induce directional recrystallisation. In this way, if a given combination of specimen travel speed and peak temperature results in a value of kinetic strength which is less than D_E, then those conditions should not lead to complete recrystallisation. An excess of kinetic strength beyond D simply should lead to additional annealing after recrystallisation is completed. The concept is illustrated in figure 6.2, where treatment 2 has just the right kinetic strength to induce directional recrystallisation, whereas, treatment 1 and 3 are inadequate and excessive, respectively.

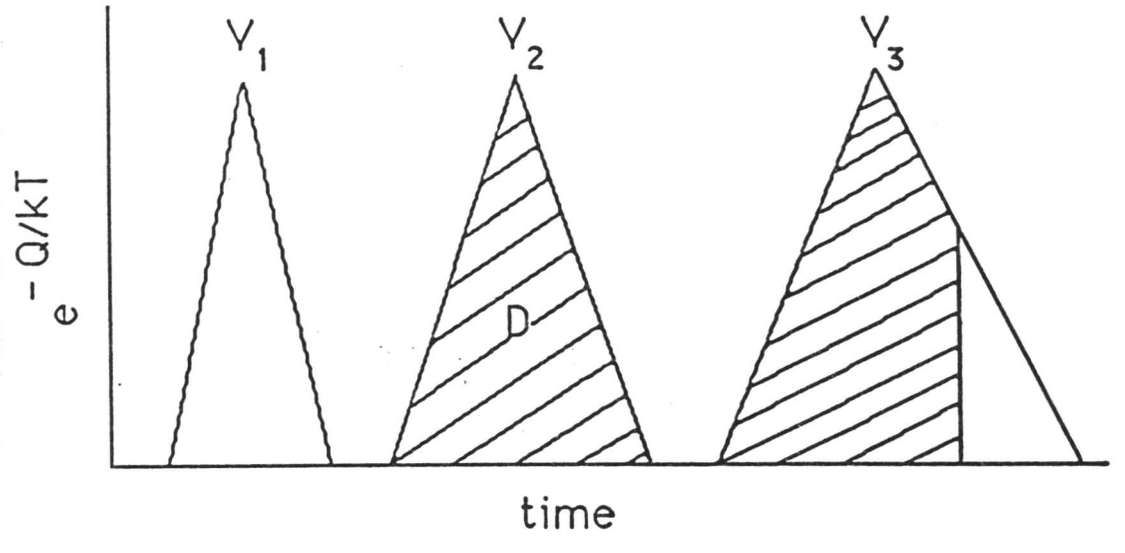

Figure 6.2. Illustrate the concept of "kinetic strength" D as discussed above.

The kinetic strength may be expressed mathematically as:

$$D = \int_{t_0}^{t_1} \exp\left\{-\frac{Q}{RT}\right\} dt \qquad \text{.....(6.4)}$$

The transition from partially recrystallised to a fully recrystallised sample should then occur when D achieves a critical value $D = D_E$.

A further useful concept is the effective temperature T_E associated with the heat treatment. It can be derived as illustrated in figure 6.3 by converting the anisothermal heat treatment into an isothermal treatment while maintaining the value of D.

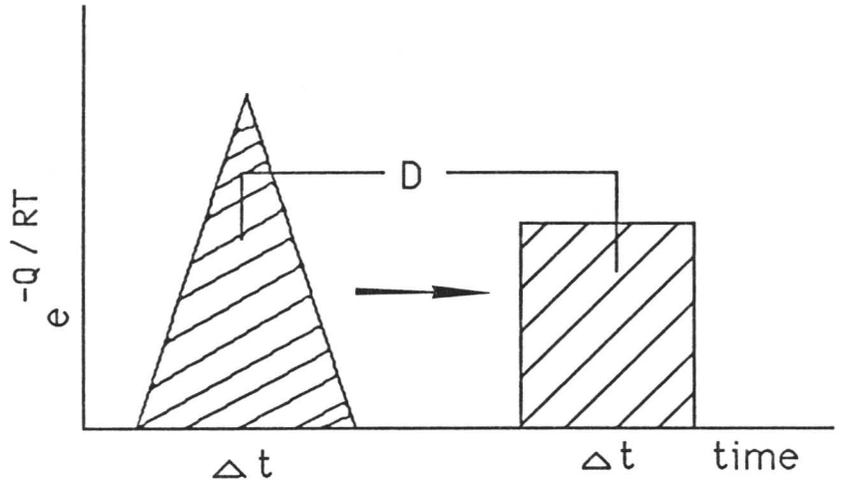

Figure 6.3. Illustrate the concept of effective temperature T_E associated with the heat treatment, by coverting the anisothermal heat treatment into an isothermal treatment while maintaining the value of D. It follows that the minimum effective temperature is given by

$$T_E = -\frac{Q}{R}\ln\left\{\frac{D_E}{\Delta t}\right\} \qquad .....(6.5)$$

The effective temperature T_E also permits an experimental evaluation of the value of the unknown activation energy Q. Zone annealing experiments can be carried out at two peak temperatures and variety of specimen travel speeds.

These should yield two interface velocities at different effective temperatures, the velocity in each case determined by the speed at which a transition from directional recrystallisation to partial recrystallisation is achieved. It follows that,

$$\frac{V_2^A}{V_2^B} = \exp\left\{-\frac{Q}{R}\left(\frac{T_E^A - T_E^B}{T_E^A\, T_E^A}\right)\right\} \qquad .....(6.6)$$

where,

V_2^A specimen travel speed at the transition from fully recrystallised to partially recrystallised samples, during zone annealing with a peak temperature "A"

V_2^B specimen travel speed at the transition from fully recrystallised to partially recrystallised samples, during zone annealing with a peak temperature "B"

T_E^A effective temperature associated with zone annealing in which the peak temperature is "A"

T_E^B effective temperature associated with zone annealing in which the peak temperature is "B".

By identifying the transition from fully to partial recrystallisation for two peak temperatures, equation 6.6 can be solved to yield a value of the activation energy. Experimental data (figure 6.4) were obtained from zone annealing experiments at peak temperatures of 1150 and 1380°C, and were used to evaluate the activation energies. Three (at T_p = 1180 - 1280°C) transition points have been used to measure the average value of Q. The first transition was taken from the results obtained after zone annealing specimens at 1200°C with specimen travel speed 1.4 mm/min. The second and third transition were taken from 1280°C (7.7 mm/min) and 1180°C (1.4 mm/min) respectively.

The measured value of the activation energy Q was found to be 402791 J mol^{-1} which is much larger than the corresponding activation energy for self diffusion in α-iron (Q = 257500 J mol^{-1} as reported by Weast, 1976-77). The value is probably much higher because of the particle dispersion present in the samples or as a consequence of some kind of a solute drag effect.

The graphs have been plotted as a function of time and temperature for the data measured during operation at the temperatures ranging from 1150 to 1380°C, with different specimen travel speeds are shown in figure 6.4. By integrating the same data graphs have also been plotted for exp(-Q/RT) versus time (figure 6.5).

The area under the curve (D) have been calculated from the graphs shown in figure 6.4 by using measured value of Q (402791 J mol^{-1}). From the values of D, calculated for different temperatures and specimen travel speeds, graphs have been plotted for the integral D (seconds) versus velocity (mm/min) and are shown in figure 6.6, where a band has been drawn within the values of the transition from directional recrystallisation to partially directional recrystallisation.

It was hoped that the transition for directional recrystallisation to partial directional recrystallisation would fall within the same value of kinetic strength irrespective of temperature. This is in fact the case for all samples except those annealed at lowest temperature for which the results do not fit the theoretical approach. The results are consistent with the theory except in the case of zone annealing experiments at T_p = 1150°C. Discrepancies probably arise because nucleation is difficult at this temperature.

The degree of recrystallisation can be estimated from the hardness data for the specimens which recrystallised partially:

$$\% \text{ recrystallised} = [1 - \{(H - H_{min}) / (H_{max} - H_{min})\}] 100$$

where H is the hardness of the partially recrystallised sample, H_{max} is the hardness of the sample in deformed condition and H_{min} is the hardness of a fully recrystallised sample. The results are illustrated in figure 6.6.

6.6 Further Experiments

From figure 6.12 and Table 6.3, it can be seen that at T_p = 1280°C for the 0.8 - 5.0 mm/min specimen travel speeds there is little correlation between grain size and specimen travel speeds. However, as the speed increases further, the grain width is found to increase sharply. This could be attributed to the fact that at high temperatures where grain boundary mobility is also high, any differences in mobilities will lead to the dominance of the grains with highest growth rates.

To check whether the recrystallisation front tends to be ragged, as would be expected when there are differences in grain boundary mobilities, some specimens were deliberately partially recrystallised. Figure 6.14, shows the microstructure recorded from the samples zone annealed at T_p = 1280°C, with the samples being rapidly quenched in water when the region illustrated entered the R. F. coil. It is very clear that the recrystallisation front is far from uniform, with significant differences in the penetration of grains into the deformed region.

An attempt was also made to directionally recrystallise specimens prepared with the zone annealing direction perpendicular to the rolling direction, at peak temperatures ranging from 1180 to 1380°C and using specimen travel speeds of 1.4, 3.2 and 5.0 mm/min (Figures 6.15 - 17). The samples often recrystallised only partially and with more or less equiaxed grain growth. The specimens were only nominally effected by the temperature gradient. At the highest peak temperatures (1280 and 1380°C), directional recrystallisation did occur, but in the wrong direction, parallel to the deformation direction rather than the zone annealing direction.

This kind of recrystallisation behaviour has been only detected in this alloy (MA956), and reveals the influence of hot rolling and particle alignment on the recrystallisation in MA956. The transmission electron micrograph (figure 6.18) provides an evidence for the particle alignment along the direction of the hot rolling.

Symbols	Terms
D	As-deformed
DX	Directionally recrystallised
HV	Vickers hardness
PDX	Partial directionally recrystallised
Pl: RD	Parallel to the rolling direction
Pr: RD	Perpendicular to the rolling direction
T_p	Peak temperature
PX	partially recrystallised
X	Recrystallised with an equiaxed grain structure.

Table 6.2a. Microstructure and Vickers hardness data obtained for Incoloy alloy MA956, after zone annea
and specimen travel speeds. HV in the as-received condition was 350 HVN(10kg).

T_P °C	Specimen	Specimen Travel Speed mm/min						Hardness Vickers HVN(10kg)						Mear
	Condition	0.2	0.4	0.8	1.4	3.2	5.0	0.2	0.4	0.8	1.4	3.2	5.0	0.2
1150	Pl: RD	PDX	PDX	D	D	D	D	306	327	319	327	333	333	322
								319	322	330	327	333	330	
								333	330	330	325	336	333	
								327	325	327	325	330	333	
								325	325	322	325	330	333	
1180	Pl: RD			DX	PDX	PDX	D			258	283	339	339	
										258	333	345	348	
										258	235	339	348	
										258	294	345	342	
										258	285	339	345	
1180	Pr: RD				X	PX	PX				274	329	310	
											309	325	325	
											306	330	342	
											292	330	333	
											281	333	306	

Table 6.2b. Microstructure and Vickers hardness data obtained for Incoloy alloy MA956, after zone annealing at dif
specimen travel speeds.

T_P °C	Specimen	Specimen Travel Speed mm/min							Hardness Vickers HVN(10kg)							Me
	Condition	0.4	0.8	1.4	3.2	5.0	7.7	10.0	0.4	0.8	1.4	3.2	5.0	7.7	10.0	0.4
1200	Pl: RD	DX	DX	PDX	PDX	D	D	D	287	289	325	333	339	342	348	288
									283	292	330	336	336	348	345	
									304	314	336	339	342	363	342	
									285	304	333	339	333	348	339	
									281	229	317	342	319	342	342	
1280	Pl: RD		DX	DX	DX	DX	PDX	PDX		245	256	276	272	281	317	
										258	262	270	276	281	325	
										258	262	276	287	279	322	
										253	256	264	262	276	283	
										258	254	270	262	270	279	
1280	Pr: RD			X	DX	DX					279	268	264			
											274	270	272			
											292	262	272			
											264	264	272			
											268	263	262			

Table 6.2c. Microstructure and Vickers hardness data obtained for Inconel alloy MA956, after zone annea
specimen travel speeds.

T_P °C	Specimen	Specimen Travel Speed mm/min						Hardness Vickers HVN(10kg)						M
	Condition	0.8	1.4	3.2	5.0	7.7	10.0	0.8	1.4	3.2	5.0	7.7	10.0	0
1380	PI: RD	DX	DX	DX	DX	DX	DX	247	253	245	264	254	270	2
								251	251	242	258	266	274	
								254	245	285	256	276	272	
								262	249	270	245	283	262	
								225	247	266	249	274	268	
1380	Pr: RD	X	DX	DX	DX	X	X	243	258	254	258	247	254	2
								233	249	254	260	253	274	
								233	245	253	264	249	281	
								233	249	253	268	251	276	
								227	238	245	251	254	245	

6.7 Isothermal Annealing of ODS Alloy MA956

Isothermal annealing experiments were performed on oxide dispersion strengthened ferritic stainless steel MA956 (for chemical composition see Table 6.1 & 3.1), using conventional resistance furnaces. The specimens were annealed isothermally at temperatures ranging from 1160 to 1360°C, at 100°C intervals. The annealing time was initially 900 seconds, the time period being doubled for each successive heat treatment, to maximum of 57600 seconds. The hardness (HVN) data for the annealed samples are listed in Table 6.4 and are graphically shown in figure 6.19.

Figure 6.20 illustrate the microstructure recorded after successive annealing treatments at 1160°C. It is evident that even for the maximum annealing time (57600 seconds), the specimen is not fully recrystallised; only a few grains can be seen growing from the edges of the sample. As the annealing time was increased the volume fraction of recrystallised grains was seen to increase. The hardness measurements (Table 6.4) are consistent with the observations that the annealing treatments at 1160°C, lead to fully recrystallised specimens.

If the hardness values and microstructural results of the specimens isothermally annealed at 1260 and 1360°C are compared with those obtained after annealing at 1160°C (figures 6.20, 6.21 and 6.22), which represents the microstructure recorded after isothermal annealing the samples at 1260 and 1360°C, then it is once again clear that the heat treatments at 1160°C are inadequate to produce full recrystallisation.

Equiaxed grains were never detected during isothermal annealing, the recrystallised grains being columnar along the deformation direction. The formation of columnar grains in unidirection is possibly due to the alignment of particles, as has been already discussed in zone annealing section of MA956. These results contrast with the observations on the superalloy, where isothermal annealing gave equiaxed grains. Assuming that in the case of the nickel base superalloy secondary recrystallisation occurs when the alloy is zone or isothermally annealed, whereas with the steels, it is primary recrystallisation. The driving force for change during annealing of the as-received material is therefore expected to be much smaller with the superalloy. This may be the reason why isothermal annealing only produces equiaxed grains for the superalloy but directionally recrystallised grains for steel (MA956).

6.8 Conclusions

The directional recrystallisation behaviour of alloy MA956 appears to be strongly influenced by its manufacturing process. In particular, the oxide dispersoids seems to align along the "hot" working direction. This alignment, which has been demonstrated to favour anisotropic grain growth along that direction, even when the imposed temperature gradient is not parallel to the working direction.

The behaviour of the alloy during anisothermal annealing can be rationalised approximately, using concept of "kinetic strength". Measurements of grain boundary velocities under different zone annealing conditions enabled the estimation of the activation energy governing grain boundary mobility. The activation energy is significantly higher than that for self diffusion in iron, perhaps because of the effects of particles in pinning the boundaries, or as a consequence of some kind of a solute drag effect.

Similar microstructures of directionally recrystallised columnar grains were always observed irrespective of the isothermal heat treatment applied. Equiaxed grains were not detected for this alloy (MA956), for any of the isothermal heat treatments considered in the present work. The microstructural results obtained after isothermal annealing at the range of temperatures and over a variety of periods of time provides further evidence of the influence of oxide particle alignment on the recrystallisation behaviour of alloy MA956.

Table 6.3. Grain size measured by linear intercept method, after zone annealing MA956 at different temperatures and specimen travel speeds. The values given in brackets indicate the standard deviation of the measurements.

Material	T_p	Specimen travel speed mm/min					
	°C	0.8	1.4	3.2	5.0	7.7	10.0
		Grain size (G') mm					
MA956	1180	0.09					
		(0.05)					
	1280	0.17	0.14	0.17	0.14		
		(0.05)	(0.05)	(0.05)	(0.05)		
	1380	0.12	0.14	0.17	0.12	0.13	0.30
		(0.05)	(0.05)	(0.05)	(0.05)	(0.05)	(0.08)

Table 6.4. Hardness (HVN) data obtained after isothermal annealing of MA956 at different temperatures and for a variety of time periods.

Temperature	Annealing time in seconds						
°C	900	1800	3600	7200	14400	28800	57600
	Hardness HVN(10kg)						
1160	343	321	335	319	321	305	308
	341	333	325	325	331	308	319
	339	333	329	325	323	310	323
	339	329	325	323	329	319	323
	341	325	322	322	319	305	313
	Mean hardness values						
	341	328	327	323	324	309	317
1260	323	301	277	256	262	254	246
	343	284	274	275	264	268	265
	339	296	284	284	268	271	258
	337	282	278	275	260	258	258
	333	277	284	265	260	254	265
	Mean hardness values						
	335	288	279	271	263	261	258
1360	253	264	246	246	238	246	238
	264	257	257	256	246	243	244
	256	261	265	248	250	239	237
	257	248	264	248	240	252	243
	253	257	246	246	238	246	238
	Mean hardness values						
	257	257	256	249	242	245	240